Title

5-Bev NEUTRON CROSS SECTIONS IN HYDROGEN AND OTHER ELEMENTS

Authors

Atkinson, John H.
Hess, Wilmot N.
Perez-Mendez, Victor
et al.

Publication Date

1960-11-18

UCRL -8966 Rev

UNIVERSITY OF CALIFORNIA

Ernest O. Lawrence Radiation Laboratory

BERKELEY, CALIFORNIA

DISCLAIMER

UCRL-8966 Rev.

UNIVERSITY OF CALIFORNIA

Lawrence Radiation Laboratory
Berkeley, California

Contract No. W-7405-eng-48

5-Bev NEUTRON CROSS SECTIONS IN HYDROGEN AND OTHER ELEMENTS

John H. Atkinson, Wilmot N. Hess, Victor Perez-Mendez, and Roger Wallace

November 18, 1960

5-Bev NEUTRON CROSS SECTIONS IN HYDROGEN AND OTHER ELEMENTS

John H. Atkinson, Wilmot N. Hess, Victor Perez-Mendez, and Roger Wallace

Lawrence Radiation Laboratory
University of California
Berkeley, California

November 18, 1960

ABSTRACT

This experiment measured the neutron total and reaction cross sections at 5.0 Bev. Transmission measurements were made in good and poor geometry. The high-energy neutron beam was produced when the Bevatron circulating proton beam struck a copper target. Neutrons were identified by their production of pions in a beryllium block. The pions were then detected by a counter telescope including a gas cerenkov counter. The threshold of this gas cerenkov counter defined the mean effective neutron energy at 5.0±0.4 Bev, with the half-intensity points of the neutron energy distribution at 5.9 and 4.2 Bev. The cross sections measured for the various elements are (in millibarn):

	Pb	Sn	Cu	Al	C	H
σ_t	2534±105	1986±88	1158±34	614±33	319±20	33.6±1.6
σ_r	1670±79		586±25	381±27	235±16	

The 5-Bev total cross sections are 20% below the total cross sections measured at 1.4 Bev by Coor et al.,[1] whereas the reaction cross sections remain essentially constant as a function of energy above 300 Mev. This behavior of the cross sections can be interpreted by a generalized diffraction theory developed by Glassgold and Greider.

5-Bev NEUTRON CROSS SECTIONS IN HYDROGEN AND OTHER ELEMENTS

John H. Atkinson, Wilmot N. Hess, Victor Perez-Mendez, and Roger Wallace

Lawrence Radiation Laboratory
University of California
Berkeley, California

November 18, 1960

I. INTRODUCTION

At 1.4 Bev the neutron total cross sections are rising with energy. Robert Williams made the prediction, based upon these data and some high-energy cosmic-ray data, that the nucleon-nucleon total cross section would be found to rise monotonically from 42 mb at 1.4 Bev to 120 mb at 30 Bev.[2] This prediction came into question with the publication of the high-energy p-p elastic scattering data of Cork, Wenzel, and Causey, which showed a decrease in the elastic scattering cross section from a peak value at 1.5 Bev.[3] In the present experiment in order to extend neutron cross sections to higher energies, the total and reaction cross sections were measured for 5-Bev neutrons in lead, copper, aluminum, and carbon to an accuracy of about 5%. The total n-p cross section was measured directly in liquid hydrogen.

The gas cerenkov counter used in this experiment limits the effective neutron energy to a minimum of 3.5 Bev while the maximum energy available was the 6.2-Bev peak energy of the Bevatron. Knowledge of the neutron energy is critical for determining meaningful cross sections, and is quite difficult to achieve with high-energy neutron beams.

The experiment is interpreted by a new theory developed by Glassgold and Greider to interpret high-energy scattering data.[4] This generalized diffraction theory gives expressions for the total and reaction cross sections in easily calculated closed forms that fit the neutron scattering data well

from 300 Mev to 5 Bev. A simple optical model has also been fitted to our data, giving a check on our energy determination as well as the usual optical-model parameters.

II. EXPERIMENTAL METHOD

A. Experimental Arrangement

1. Beam

The neutron beam was generated by the Bevatron internal proton beam striking a 1/2×1/2×3-in. copper target with the 3-in. dimension tangent to the circulating proton beam. Whenever the primary proton beam was spilled on a target, neutrons were produced in the forward direction which for this experiment were used at 0 degrees from the target, since there is a maximum neutron flux and energy in the forward direction. The neutrons emerged from the north straight section of the Bevatron with a 4-in. path length in the steel structure of the tangent tank. The neutron beam was collimated as it passed through the Bevatron shielding wall by a 2×2×60-in. aperture in 5 ft of lead located 45 ft from the Bevatron target, subtending a half-angle of 0.1 14 degrees. Two 1-in. lead bricks 6 in. apart in the mouth of the collimator were an effective γ-ray filter, since the stray field of the Bevatron sweeps away all electrons thus produced.

2. Monitor

The Bevatron proton beam flux is highly variable from pulse to pulse. Comparison of successive runs required an accurate monitor to count at a rate proportional to the high-energy neutron flux in the channel. The monitor consisted of a gas cerenkov counter followed by two 4×4-in. plastic scintillators, operating in triple coincidence. This assembly, shown in Fig. 1, was placed immediately after the collimator, directly in the path of the neutron beam. The cerenkov counter contained Freon-12 (CCl_2F_2) at 15 psig and

counted charged pions of energy greater than 2.4 Bev produced in the γ-ray filter lead bricks at the entrance of the collimator and in the walls of the collimator. The two plastic scintillators determined the geometry of the monitor telescope and eliminated accidental counts through the requirement for a triple coincidence. The last element of the monitor was 18 ft from the γ-ray filter, from which it subtended a half-angle of 0.53 deg, and was 63 ft from the Bevatron target, from which it subtended an angle of 0.152 deg. The monitor and the neutron detector being 24 ft apart, allowed both good- and poor-geometry absorber positions.

3. Detector

The neutron detector illustrated in Fig. 1 consisted first of a 6×6×1-in. plastic scintillation counter connected in anticoincidence to the neutron coincidence circuit. This counter eliminated detector counts from charged particles in the beam. Its large size, as compared with the 2×2-in. beam cross section, reduced background caused by charged particles scattering into later elements of the anticoincidence counter.

Following the anticounter, the neutrons generated charged pions in a 12×2×2-in. beryllium block. For some poor-geometry measurements, an 8×2×2-in. aluminum block was substituted because of its shorter length. Beryllium is a more efficient pion generator than aluminum, having a large cross section for inelastic neutron events and a low total cross section for the pions thus produced. The maximum efficiency estimated for producing detectable pions was 0.38 for 12 in. of beryllium and 0.25 for 8 in. of aluminum. In calculating these efficiencies, it is assumed that all inelastic neutron events in the converter produce high-energy pions in the forward direction. The pions produced are considered lost if they interact or scatter

in leaving the converter.

A 2×2×1-in. plastic scintillator following the converter was connected in coincidence with the two following counters in the detector. This counter, in conjunction with the converter, determined the geometry of the measurement.

Charged pions of sufficient energy were then detected by a 10-in. diam gas cerenkov counter similar to the monitor cerenkov counter described elsewhere.[5] The gas cerenkov counters were energy threshold detectors and, together with the neutron spectrum, placed a lower limit on the effective neutron energy. Protons did not count, since their β was below the threshold of the cerenkov counter. The detector cerenkov counter was filled with Freon-12 (CCl_2F_2) at 30 psig. This gave an absolute energy threshold of 1.56 Bev for charged pions. However, the threshold efficiency of the counter was not a steep function and the minimum effective pion energy was 1.85 Bev for 50% counting efficiency. From the minimum pion energy, a minimum energy for the neutrons that produced them is derived. The effective energy distribution of the neutrons is discussed in Section II-B.

Another detector element is necessary. Neutral pions were produced in the converter with a relative multiplicity of about 1/3. The neutral pions decayed, essentially where they were produced, to two gamma rays. Some of these gammas then produced electron pairs in the converter. These electrons could be counted by the following scintillation counters and the gas cerenkov counter. This would destroy the energy discrimination of the detector since even a 15-Mev electron would have been counted. To preserve the energy discrimination of the detector, an electron filter was placed behind

the 2×2-in. geometry-defining counter but ahead of the cerenkov counter. This filter consisted of 2 inches of lead (10 radiation lengths) plus an inch of iron which also served as a magnetic shield for the counter near the 6-kilogauss magnetic sweeping field. From approximation shower theory the average energy of the electrons emerging from the lead is given by $E = E_0 2^{-10}$. For a 2-Bev neutral pion this gives an approximate electron energy of 1 Mev. The 6-kg field applied over 2.5 cm swept all electrons of energy less than 87 Mev out of the cerenkov counter while deflecting the charged pions less than 1 deg. In this way π^0 electrons were effectively prevented from counting in the detector.

4. Electronics

The electronic components employed were conventional high-speed counting devices and are illustrated in Fig. 5. Hewlett-Packard prescalers were used in the monitor to permit counting without jamming during the rapid-beam-ejector pulse of 300 μsec required by the concurrent bubble chamber experiment.

We required especially stable discrimination levels since the effective energy threshold of the cerenkov counters depends upon the size of signal required to register as a count. A stable discriminator amplifier developed for the purpose[6] was used to establish the discrimination levels, which were set so that the scalers would just count with a 2.8-volt signal from a mμsec pulser put into the coincidence circuits. The 2.8 volt level chosen was the mid-point between the tripping level and saturation for the Evans coincidence circuits employed. The actual counter signals exceeded 5 volts in normal operation. The discriminator amplifiers were very stable in operation, requiring a correction not exceeding 0.05 in an average week of operation.

B. Neutron Energy

The effective neutron energy was determined by the energy selectivity of the neutron detector and by the incoming neutron energy spectrum. The effective neutron energy distribution is illustrated in Fig. 3. Analysis of this skew distribution gives the peak at 5.25 Bev with the half-intensity points at +0.65 Bev and -1.0 Bev. From numerical integration of the spectrum the mean energy is found to be 5.0 Bev with the probable error points at ±0.4 Bev. This distribution is derived by folding together the primary neutron spectrum from the Bevatron, the energy distribution of pions from the converter for several pion-production multiplicities, and the energy-sensitivity curve of the cerenkov counter, each with its appropriate weighting factor.

The spectrum of the primary beam of neutrons coming from the Bevatron was roughly measured by Holmquist with a hydrogen-filled diffusion cloud chamber.[7] He found a distribution peaked at 3.8 Bev and decreasing to zero at 6.2 Bev. His spectrum has been corroborated by the work of Barrett with Bevatron neutrons in emulsion.[8] Rough values for pion multiplicities from n-p scattering, and the pion energy spectrum in the forward direction, are also given by Holmquist.

The assumptions and the models used in deriving this energy distribution are admittedly crude. Fortunately, the mean effective neutron energy, the parameter of importance in the cross section measurement, is not very sensitive to this derivation since the cerenkov counter threshold is the determining factor in the energy selection. The mean energy derived in this way is the energy expected from a very rough consideration of the 6.2-Bev upper limit of the Bevatron energy and the 3.5-Bev lower limit of the cerenkov counter threshold modified by the increased efficiency of the cerenkov counter at higher energies.

A completely independent determination of the mean energy from the optical model of the nucleus is discussed in Section IV B, which gives a value of 5.3±2.3 Bev.

C. Counting Rates

We employed only "left-over" beam available from concurrent experiments, so counting rates were quite low and were the limiting factor in both the accuracy and the extent of the experiment. The neutron counting rate with no absorber averaged 10 counts per minute, but varied from 1 to 100 counts per minute depending upon the Bevatron beam levels and target configurations for the other experimenters. The monitor counted at a rate approx 100 times that of the neutron detector.

Barrett measured a neutron flux at the Bevatron with nuclear emulsions and calculated the source strength of the neutrons as 0.19 neutron per steradian per proton striking the target.[8] Obstructions in the neutron beam path for our experiment, including the lead γ-ray filter and the steel of the tangent tank frame, leave a neutron transmission of 30%. The detector subtends the very small solid angle of 3.76×10^{-6} steradian at the Bevatron target. Finally, the detector efficiency is calculated to be approximately 0.4%. Combination of these factors for neutron production rate, attenuation, solid angle detected, and detection efficiency gives a calculated counting rate of 10 counts per 10^{10} protons on the target. The counting rate predicted by using Barrett's measured source strength agrees within an order of magnitude with our observed rate.

III. RESULTS

A. Cross-Section Measurements

1. Transmission Measurement

This experiment was basically a simple transmission measurement in good geometry (approx 0.2 deg) and in poor geometry (4 deg). For lead and for carbon the integrated cross section was also measured as a function of the half-angle subtended by the detector (converter). Angles of the first diffraction minima vary with element from 1 deg to 2 deg, making all the angles of interest quite small. Angles of the first diffraction minima for the elements measured are given in Table I, as calculated on the opaque circular cylinder model, which gives

$$\theta_m = 0.61 \frac{\lambda}{R} = 0.61 \frac{h}{pR} = 0.61 \frac{h}{p(1.28\, A^{1/3} \times 10^{-13})} ,$$

where θ_m is the half-angle of the first minimum, p is momentum, and A the mass number of the absorber atoms.

The two absorber thicknesses used were generally 0 and approx a half absorption length in the element being measured. These lengths gave an appreciable transmission difference while minimizing multiple-scattering problems. The number of neutrons transmitted is given by

$$N = N_0 e^{-n\sigma x} .$$

All symbols have the usual meaning. The log of the ratio of detector counts, N, to those of the monitor, M, is then given by

$$\ln r = \ln \frac{N}{M} = -n\sigma\, \theta + \ln C,$$

where C is a constant relating the number of neutrons N_0 in the unattenuated beam to the monitor counts.

The slope, $-n\sigma$, of the plot of ln r vs x is evaluated by least-squares fitting, with proper attention given to the weighing of the datum values of ln r. The data illustrated in Fig. 4 for several thicknesses of lead are fitted well by a straight line.

2. Geometric Corrections

Since the angles related to the diffraction pattern are small (as discussed above), the finite sizes of the beam and the converter complicate the definition of the angle subtended by the detector. A geometric correction for the finite beam size was made as follows: The diffraction pattern for an opaque disc of radius R is given by

$$\frac{d\sigma_d}{d\Omega} \sim \left[\frac{J_1(kR \sin\theta)}{\sin\theta}\right]^2, \qquad (1)$$

where $d\sigma_d/d\Omega$ is the differential elastic scattering cross section, J_1 is the first-order Bessel function and k is the neutron wave number. This is close to the scattering from an opaque sphere for $kR > 1$, where k is the absorption constant of the optical model discussed in Sec. IV-C. Values of kR for this experiment range from 2.98 (lead) to 1.16 (carbon).

The partially integrated elastic scattering cross section is defined as

$$\sigma_d(\theta) = \int_0^{\theta} \frac{d\sigma_d}{d\Omega}\, \Omega d. \qquad (2)$$

A mean $\sigma_d(\theta)$ for a finite beam size may be defined as

$$\overline{\sigma_d(\theta)} = k \int_{A_1} \int_{A_2} \frac{J_1(k\,R\,\sin\theta)^2}{\sin\theta} \frac{dA_1}{l^2} \frac{dA_2}{A_2}, \qquad (3)$$

where areas A_1 and A_2 represent the midsections of the absorber and the converter respectively. We normalize $\overline{\sigma_d(\infty)} = 1$, and define the partially integrated differential cross section normalized to unity as

$$F(\theta) = \frac{1}{\sigma_d} \int_0^{\theta} \frac{d\sigma_d}{d\Omega}\, d\Omega. \qquad (4)$$

Then $\sigma(\theta)$, the cross section determined by the transmission with a given subtended angle θ, is related to the reaction cross section σ_r and elastic cross section σ_d by

$$\sigma(\theta) = \sigma_r + \left[1 - F(\theta)\right] \sigma_d \qquad (5)$$

$$= \sigma_r + F'(\theta)\, \sigma_d.$$

We measure $\sigma(\theta)$ by this experiment for several values of θ. $F(\theta)$ has been calculated by a computer code evaluation of Eq.(4). Then a least squares fit of the linear form of Eq.(5) gives σ_r as the intercept (a) and σ_d as the slope (b) of the straight line.

The corrections for the finite beam size raise the total cross section as much as 5% for lead and decrease the reaction cross section as much as 10% for carbon.

The above correction assumed that all scattered neutrons were scattered at the midplane of the absorber and produced pions in the midplane

of the converter. A small correction was made for this by integrating along the beam direction Z. The finite length of the absorber again makes θ, the angle subtended by the detector, indeterminate. However, this effect averages out, since sin θ is linear for the small angles involved. The converter efficiency W varies slowly with length and is given by

$$W = \left[\exp(-Z/\lambda_n) - \exp(-Z/\lambda_\pi)\right] / \left[(\lambda_\pi - \lambda_n) - 1\right],$$

where λ_n is the inelastic interaction length for neutrons in beryllium and λ_π is the total interaction length for pions in beryllium. The sensitivity of the detector is assumed to be constant for the scattering angles possible in this experiment. The cerenkov counter accepts less than a 3-deg cone, and the pion angular distribution is flat over these small angles, as is indicated in the Holmquist[7] and Brookhaven[1] papers.

3. Results

The results of all the transmission measurements for all angles measured and for all elements measured are given in Table II. Table III gives the total (σ_t), reaction (σ_r), and elastic (σ_d) cross sections derived from these measurements and compares them with two commonly used geometric cross sections. Figures 5 through 8 illustrate the least-squares fits corrected to the experimental data.

B. Errors

1. Beam Contamination

Contamination of the neutron beam with charged particles or other neutral particles could give errors in the cross section measurements.

However, charged particles generated in the Bevatron target are swept out by the Bevatron magnetic field before reaching the collimator, while scattered charged particles are swept out by the fringing field. Measurements with the counter telescopes indicate that the effects of charged-particle contamination are negligible.

High-energy gamma rays are produced in the Bevatron target in numbers comparable to the number of neutrons produced. However, they must pass through 4 in. of steel and 2 in. of lead before reaching the monitor counters. This 16 radiation lengths of material greatly reduces the number and energies of the gamma rays. Further, in order to introduce a serious error the gammas would have to produce neutrons in the absorber, or charged pions in the converter, since an effective electron – gamma-ray filter follows the converter. These are unlikely, and gamma rays were not a problem. Neutral pions likewise decay immediately into two gamma rays and are similarly eliminated.

All the neutral strange particles, excepting the long-lived component of the neutral K particles, have lifetimes shorter than 10^{-10} sec and cannot traverse the 86-ft path length of this experiment. The K^0_2 has a mean life of approximately 10^{-7} sec and could possibly cause trouble. However, K^0 mesons are produced at only about 10^{-4} the rate of neutrons in the Bevatron target.[9] Half of those produced decay quickly by the K^0_1 mode, and the K^0_2 mode regenerates K^0_1 mode particles in interactions in the 4 in. of steel and 2 in. of lead in the beam, further reducing the K^0 flux by decay through the K^0_1 mode. Finally, K^0 mesons do not have radically different cross sectons from neutrons, making very small contaminations unimportant. Thus beam-contamination errors are unimportant compared with the general

accuracy of this experiment.

2. Geometry

Because of the very small angles involved in this experiment, geometric corrections are important. The geometry of the primary neutron beam is well defined, since the distances are large between the target and the relatively small detector elements. The neutron beam is defined to a half-angle of 0.1 14 deg by the collimator, 0.152 deg by the monitor, and 0.0556 deg by the neutron detector (converter). However, the lead gamma-ray filter in the mouth of the collimator acts as a diffuse source of elastically scattered neutrons.

Elastically scattered neutrons from the 2-in. lead gamma-ray filter comprise 20% of the neutron beam on the basis of our measured value of σ_d. The gamma-ray filter is 18 ft from the good-geometry absorber position and the absorber subtends an angle of 0.53 deg. Since the diffraction pattern minimum for elastically scattered neutrons from lead is at 1 deg, approximately 75% of the neutrons are scattered through angles less than 0.53 deg. Half of these neutrons scatter toward the central ray and thus possibly into the neutron detector. The change in cross section resulting from a change in the subtended angle of the good-geometry position from 0.2 deg to 0.5 deg may be estimated (from the variation of integral cross section as a function of angle, illustrated in Fig. 5) as 20%. These estimates give a combined error of 1.5%, which is not significant in comparison with the statistical uncertainties of the experiment.

Corrections for alteration of the diffraction pattern by the finite beam size were made in Section III A2. Since these corrections are a maximum of 10%, a 10% error in the model used for the correction would give a cross section error of 1%. Since the model used applies well for Kr>1

and our values of KR range from 1.16 to 2.98, the error from this correction should be much less than 1%.

In poor geometry, neutrons from some inelastic events are also collected. This problem was considered by Cronin et al. for a high-energy pion-scattering experiment.[10] The cross section measured at a given subtended angle θ is given by

$$\sigma(\theta) = \sigma_r + F'(\theta)\,\sigma_d - \int_0^{\theta} \left[\frac{d\sigma_r(\theta)}{d\Omega}\right] d\Omega. \qquad (6)$$

This differs from Eq.(5) only by the subtraction of the last term, which is the correction for inelastic events counted.

The differential reaction cross section, which gives the number of high-energy neutrons inelastically scattered into unit solid angle, may be expanded in a cosine series:

$$\left[\frac{d\sigma(\theta)}{d\Omega}\right]_r = \Sigma_n \left|a_n\right| \cos^n\theta. \qquad (7)$$

Then if the reaction cross section, σ_r, is extrapolated linearly from 7.5 deg and 15 deg the error is less than 2% when this is compared with the form of Eq.(7) for $n \leq 12$. The angles on which our values for σ_r are based are on the order of 4 deg, so that the value of σ_r may be assumed to project linearly to 0 deg. The measured cross section may be given by an expansion of Eq.(6) as

$$\sigma(\theta) = \sigma_r + F'(\theta)\,\sigma_d - 2\eta(1-\cos\theta),$$

where η is less than σ_r. Since cos 4 deg is 0.998, the correction is less than 0.2% even if all the inelastic events give high-energy neutrons in the forward hemisphere.

3. Bevatron Proton Beam Tracking

By far the largest error in the operation of this experiment came from tracking variations of the Bevatron internal proton beam. As the absorber and converter configuration was changed hourly, variations in the measured rates averaged out with many runs. Also, only internally consistent rates were combined with one another to derive a cross section. The statistical criterion of Rossini and Deming, which requires each point plus two standard deviation to overlap the mean plus two standard deviations on the mean,[11] was used to test consistency. Cross sections derived independently from each consistent set of rates were then combined to give the quoted cross section. The statistical considerations discussed in the next section (III-B4) establish that these procedures made the error from internal proton-beam variations much less than the counting statistics error.

4. Counting Statistics and Total Error

The low counting rates make statistical errors the chief limitation to accuracy in this experiment. Because of the logarithmic relationship of the cross section to the measured counting rates, the error in the measured rates must be less than 1% in order to limit the error in the cross section to 5%. Since there are no known systematic errors greater than 1%, the quoted errors are statistical. The following considerations indicate that this is a reasonable estimate of the total error of the experiment.

Most of the rate data and cross sections were sorted and combined as consistent data by using the criterion of Rossini and Deming.[11] However, all data were also combined to give means, and calculated for inconsistent data. The means derived were the same within the errors on each mean whether the data were all combined as inconsistent data or sorted for

consistency. The use of sorted internally consistent data usually resulted in smaller errors. A comparison of the independently calculated cross sections with the normal distribution expected for the quoted error indicates that the data for most elements are grouped better than one would expect for a normal distribution. Thus the random-rate variations due to Bevatron operating conditions discussed in the preceding section (III-B3) do not affect the measured cross sections within the statistical accuracy of the experiment. Since all known systematic errors were shown in Section III-B, to be less than 1%, the statistical errors are used as an estimate of the total error.

IV. CONCLUSIONS

A. Discussion

1. Comparison with Previous Experiments

The variation with energy of the neutron total cross section for lead, copper, aluminum, and carbon is illustrated in Fig. 9. The rise in the neutron total cross sections from 300 Mev to 1.5 Bev was established in 1955 by Coor et al. with their experiment at 1.4 Bev, and later data at lower energies confirm this behavior. Our values for the neutron total cross section show a consistent and substantial drop from the Brookhaven values. The high-energy cosmic ray values of Sinha and Das for the total cross section of 4-Bev penetrating secondaries in aluminum, copper, and lead[12] are somewhat lower than our values for neutron cross sections in the same elements. However, these cosmic ray cross section experiments are quite tenuous, since neither the energy nor the identity of the bombarding particles was well established.

The reaction cross section is essentially constant within the accuracy of the experiment from 300 Mev to 5 Bev for all elements measured. This is confirmed by the Brookhaven 1.4-Bev data,[1] Barrett's data at 3.6 Bev,[8] and the cosmic ray data at 4.0 Bev of Sinha and Das.[12] Thus the radical change in the total cross section must be due to a sharp drop in the elastic cross section. The theory discussed in Section IV-B relates this decrease to a decrease in the nucleon-nucleon cross section.

2. Nucleon-Nucleon Cross Sections

A liquid hydrogen target was used in this experiment to give the n-p cross section directly. The n-p total cross section shown in Fig. 10 exhibits the same drop from 1.4 to 5.0 Bev as characteristic of the heavier nuclei discussed above. The high-energy p-p elastic cross section data of Cork and Wenzel[3] also exhibit the same drop, although not so dramatically as our data. The n-p reaction cross section (nonelastic) is very difficult to measure and has not been measured above 300 Mev. The increase in the nucleon-nucleon total cross section from the low point at about 300 Mev starts at the threshold for pion production. Furthermore, the peak of the nucleon-nucleon total cross section at 1.4 Bev occurs at roughly the threshold for strange-particle production.

B. INTERPRETATION

1. Generalized Diffraction Theory

Glassgold and Greider[4] developed a generalized diffraction theory to explain the behavior of the neutron cross sections from 300 Mev to 5.0 Bev in the elements measured. This theory uses the gross-average properties of the phase shifts to magnify small changes in the reaction cross section

into large changes in the total cross section. It also crudely explains the cross sections for heavier elements in terms of the measured nucleon-nucleon cross section.

This usual expressions for the cross sections in terms of partial-wave analysis, as given by Blatt and Weisskopf,[13] are

$$\sigma_r = \pi^2 \lambda \sum_{\ell=0}^{\infty} (2\ell + 1) \left[1 - |\eta_\ell|^2 \right], \tag{8}$$

$$\sigma_t = 2\pi^2 \lambda \sum_{\ell=0}^{\infty} (2\ell + 1) \left[1 - \mathrm{Re}\,(\eta_\ell) \right], \tag{9}$$

$$f(\theta) = \frac{i}{2k} \sum_{\ell=0}^{\infty} (2\ell + 1)\,(1 - \eta_\ell)\, P_\ell\,(\cos\theta), \tag{10}$$

where σ_r is the reaction cross section, σ_t is the total cross section, λ and r are the wave length and wave number of the incoming particle, η is the complex amplitudes of the outgoing wave with angular momentum ℓ and the sum is over the ℓ partial waves. These cross sections are strictly valid only for spinless neutral particles.

The new model by Glassgold and Greider describes high-energy scattering collisions in terms of four physically significant parameters. If constant phase is assumed[14] these parameters are: L, the number of partial waves strongly absorbed; β, the opacity for small ℓ; 2Δ, the range over which the opacity function decreases from β to 0; and α, the phase of the outgoing wave. The relationship of these parameters is illustrated in Fig. 11. This model generalizes the simple diffraction theory by writing $\eta_\ell = |\eta_\ell| e^{i\alpha_\ell}$ and by assuming (a) that the interaction region can be represented as a smooth

function, i.e., that the opacity function, $1 - |\eta|^2$, decreases monotonically with l, (b) that this transition occurs mainly within an interval of width 2Δ centered about a large value of the angular momentum L, and (c) that the phase function α is continuous and vanishes for sufficiently large values of l. Several functional forms for the fall-off shape were tried by Glassgold and Grieder but the results were found to be independent of the details of this region. With these assumptions, the cross sections and scattering amplitude, as expressed in Eqs.(8),(9), and (10), can now be evaluated directly. These expressions are given in the paper by Glassgold and Greider.[4]

2. Application of Theory to Experiments

The expressions obtained in sub sec. 1 above can now be used to fit the experimental neutron-scattering data from 300 Mev to 5 Bev. Two reasonable assumptions are made: $L \propto k A^{1/3}$, where A is the atomic weight, and $\Delta \propto k$. The large variation in σ_t with energy, while σ_a remains relatively constant, requires that phase α be small, as can be seen by comparison of Eqs.(8) and (9). In fact, the best fit to the data is for $\alpha = 0$.

For small real η, σ_t varies linearly with η and is therefore more sensitive to changes in η than σ_r, which varies quadratically with η. The theoretical fit to the experimental values is given by the curve in Fig. 9. The fit is seen to be quite good, particularly when the uncertainties in the neutron cross section measurements are considered. The values of L, Δ, and β used in the analysis are given in Table IV.

Consideration of the ratio

$$\frac{\sigma_t(l)}{\sigma_r(l)} = \frac{2(1 - \eta_l)}{1 - \eta_l^2} = \frac{2}{1 + \eta_l} \qquad (11)$$

shows directly that this ratio of the total to the reaction cross section can be less than 2 as required by the data. Also this ratio decreases as η_l

increases, that is, as the opacity function $1 - |\eta|^2$ decreases. The experimental values of this ratio are given in Table V.

We can qualitatively understand β from a consideration of the nucleon-nucleon cross section. The dependence of β on k and A can be interpreted in terms of a classical picture of exponential absorption with distance, the absorption coefficient being related to the observed nucleon-nucleon total cross sections. Crudely, β is given by

$$\beta = 1 - e^{-2R \rho \bar{\sigma}_t}, \qquad (12)$$

where 2R is the maximum distance across the nucleus, ρ is the density of nucleons in the nucleus, and $\bar{\sigma}_t$ is the average nucleon-nucleon cross section. Computation of β by using our measured value of 33.6 mb gives approximate agreement with the values of β given in Table IV.

C. Optical Model

This experiment can also be analyzed in a more conventional manner by using the optical model of Fernbach, Serber, and Taylor.[15] The uniform-density model is used here for simplicity although it is no more than a first approximation. This model describes the nucleus in terms of the nuclear radius R, the absorption constant K, and k', the increment in the wave number inside the nucleus. This experiment measured σ_t, the neutron total cross section; σ_r, the neutron reaction cross sections; and the mean energy of the incoming neutrons, which gives the neutron wave number k.

In this model the absorption constant K is expressed in terms of the average nucleon-nuclear cross section and the nuclear radius R. We use our measured value of the n-p cross section (34 mb) for the average nucleon-nuclear cross section. The nuclear radius R can be derived from the reaction

cross sections for the elements measured and the average nucleon-nuclear cross section. Then k_1 is related to the known parameter by

$$\frac{\sigma_t}{\sigma_r} = 1 + \frac{2\pi}{\sigma_r} \int_0^R \left| 1 - e^{-(K+ik_1)(R^2 - r^2)^{1/2}} \right|^2 r dr. \qquad (13)$$

This expression is integrated and a value of k_1/K is then chosen which gives agreement with σ_t/σ_r for all the elements, thus determining a mean value of k_1 in terms of K. Application of Eq.(13) to our data for C, Al, Cu, and Pb gives the best fit for $k_1/K = 0.4 \pm 0.2$, although even this value is somewhat arbitrary. A least-squares fit of the data to the nuclear radii, $R = r_0 A^{1/3} \times 10^{-13}$ cm, gives a value for r_0 of 1.17 ± 0.06. A solution for the average nuclear absorption coefficient then gives $K = (5.02 \pm 0.35) \times 10^{12}$ cm^{-1}. Finally, a value of $k_1 = (0.2 \pm 0.1) \times 10^{13}$ is derived from the ratio k_1/K. The average nuclear potential is 39.1 ± 19.5 Mev. These parameters have essentially the same values as those derived by Coor et al. within the large experimental errors.

The data furnish some information on nuclear radii. The uniform density optical model gives a value of r_0 of (1.17 ± 0.06). Greider and Glassgold's diffraction theory gives values of L,[4] the number of partial waves strongly absorbed. A nuclear radius R may be defined as $L = Rk = r_0 A^{1/3} k \times 10^{-13}$. The analysis by Glassgold and Greider gives a value of r_0 of 1.26. These values are comparable to the value of $r_0 = 1.28$ which Coor et al. derived from 1.4-Bev neutron scattering and the value of the electromagnetic size of the nucleus, $r_0 = 1.19$, for an equivalent square well potential derived from electron-scattering experiments by Hofstadter.[16]

Finally, the mean energy of the incoming neutron beam may be determined from the angular half-width of the integral elastic scattering correction. This was the method used by Coor et al. to determine the mean energy of their neutron beam. For this experiment, this method gives a check on the mean energy derived from the calculated effective neutron spectrum. The data for lead are the most extensive as a function of subtended angle. The diffraction pattern for lead gives a mean neutron energy of 5.3±2.3 Bev. This compares well with the mean neutron energy of 5±0.4 Bev derived previously.

ACKNOWLEDGMENTS

We would like to express our appreciation to the many people who helped in the successful completion of this long experiment. We would like to thank Professor A. Carl Helmholz and Professor Burton J. Moyer for their support and encouragement of this experiment. Many graduate students assisted greatly in the running and analysis of this experiment.

Finally we wish to thank Dr. Edward J. Lofgren and the Bevatron crew for their courteous cooperation during the long run.

This work was done under the auspices of the U.S. Atomic Energy Commission.

REFERENCES

1. T. Coor, D. A. Hill, W. F. Hornyak, L. W. Smith, and G. Snow, Phys. Rev. 98, 1369 (1955).
2. Robert W. Williams, Phys. Rev. 98, 1393 (1955).
3. B. Cork, W. A. Wenzel, and C. W. Causey Jr., Phys. Rev. 107, 859 (1957).
4. A. E. Glassgold and K. Greider, Phys. Rev. Letters 2, 169 (1959).
5. J. Atkinson and V. Perez-Mendez, Rev. Sci. Instr. (to be published).
6. D. Swift and V. Perez-Mendez, Millimicrosecond Discriminator, Lawrence Radiation Laboratory Report UCRL-8569 (Dec. 1958).
7. Fred N. Holmquist, Pion Production in Neutron-Proton Collisions at Bevatron Energies, Lawrence Radiation Laboratory Report UCRL-8559 (Dec. 1958).
8. Paul H. Barrett, Phys. Rev. 114, 1374 (1959).
9. L. Van Rossum and L. T. Kerth, Bull. Am. Phys. Soc., Series II, 1, 385 (1956); M. Smith, H. H. Heckman, and W. H. Barkas, Composition of a Secondary-Particle Beam from the Bevatron, Lawrence Radiation Laboratory Report UCRL-3289(March 1956); W. W. Chupp, S. Goldhaber, G. Goldhaber, W.R. Johnson, and F. Webb, Nuovo cimento, N. 2, Suppl. 1, 4, Ser. X, 359 (1956). Production of K^0 mesons is assumed similar to $K^{\pm}$ production.
10. J. W. Cronin, R. Cool, and A. Abashian, Phys. Rev. 107, 1121(1957).
11. Rossini and Deming, J. Wash. Acad. Sci., 29, 416 (1939).
12. M. S. Sinha and N. C. Das, Phys. Rev. 105, 1587 (1957).

13. Blatt and Weisskopf, Theoretical Nuclear Physics, (John Wiley and Son, New York, 1954), p. 317 ff.

14. The case of nonconstant phase is discussed by Glassgold and Greider, in Generalized Diffraction Theory for Very-High-Energy Scattering, Phys. Rev. (to be published). The assumption of nonconstant phase does not affect the cross section expressions.

15. S. Fernbach, R. Serber and T. B. Taylor, Phys. Rev. 75, 1352 (1949).

16. Robert W. Williams, Phys. Rev., 98, 1387 (1955); Robert Hofstadter, Revs. Modern Phys. 28, 214 (1956); D. G. Ravenhall, Revs. Modern Phys. 30, 430 (1958).

Table I

Positions of diffraction minima

Element	First minimum		Positions (deg) at which cross sections were measured	
	$\sin\theta$	θ	σ_r	σ_t
Pb	0.0186	1° 4'	4	0.184
Sn	0.0224	1° 17'	--	0.208
Cu	0.0276	1° 35'	5	0.208
Al	0.0366	2° 6'	5	0.208
C	0.0479	2° 45'	7	0.209
H	0.1095	6° 17'	--	0.25

Table II

Measured cross sections, $\sigma \pm \epsilon$ (in mb)

L(in.)	θ(deg)	Pb	Sn	Cu	Al	C	H
320	0.179	2445±257					
312	0.184	2325±131				324±20.2	
308	0.186						
276	0.208	2445±82	1986±87.5	1097±28.1	601±29.8		
275	0.209					302±19.9	
232	0.248						33.6±1.6
114.5	0.500	1948±141					
57.25	1.00	1760±147					
36.0	1.59					292±18	
28.5	2.00	1860±224					
23.65	2.42	1684±360					
14.5	3.95					240±14.9	
14.0	4.1	1744±120					
11.5	5.0			594±24.5	435±77.7		
9.5	6.0				380±28.4		
8.94	6.38	1720±208					
8.0	7.13					268±31.3	
6.5	9.6	1725±197					

Table III

Measured total, reaction, and elastic cross section, and two common geometric cross sections for various elements (in mb)

Element	σ_t	σ_r	σ_d	$20\pi A^{2/3}$	$\pi(1.28\,A^{1/3})$
Pb	2534±105	1670±79	864±131	2190	1802
Sn	1986±88			1400	1230
Cu	1158±34	586±25	572±42	1000	817
Al	614±33	381±27	233±43	560	414
C	319±20	235±16	83.6±25.6	330	271
H	33.6±1.6			60	51.9

Table IV

Diffraction-model parameters

	Pb	Cu	Al	C
β (5 Bev)	0.94	0.94	0.93	0.89

$\Delta = 0.61\, k \times 10^{-13}$

$L = 1.26\, A^{1/3}\, k$

Table V

Ratios of total to reaction cross sections

	Pb	Cu	Al	C
$\frac{\sigma_t}{\sigma_r}$	1.51±.10	1.98±.10	1.61±.14	1.36±.13

FIGURE LEGENDS

Fig. 1. Schematic showing the experimental arrangement of the collimeter, monitor telescope, and neutron-detector telescope.

Fig. 2. Block diagram of the basic electronic components.

Fig. 3. Effective neutron-energy distribution. This distribution shows the most probable energy as 5.25±0.65 Bev and the mean energy as 5.0±0.4 Bev, where the limits on the mean energy are the probable error points. The absolute energy range is 2.1 to 6.2 Bev.

Fig. 4. Counting rate vs thickness of Pb absorber, showing the exponential decay whose slope gives the cross section.

Fig. 5. Cross section of neutrons in Pb as a function of the half-angle subtended by the neutron detector. The solid curve is a least squares fit to the data according to an opaque-nucleus calculation for a mean neutron energy of 5.0 Bev.

Fig. 6. Cross section of neutrons in Cu as a function of the half-angle subtended by the neutron detector. The solid curve is a least squares fit to the data according to an opaque-nucleus calculation for a mean neutron energy of 5.0 Bev.

Fig. 7. Cross section of neutrons in Al as a function of the half-angle subtended by the neutron detector. The solid curve is a least squares fit to the data according to an opaque nucleus calculation for a mean neutron energy of 5.0 Bev.

Fig. 8. Cross section of neutrons in C as a function of the half-angle subtended by the neutron detector. The solid curve is a least squares fit to the data according to an opaque-nucleus calculation for a mean neutron energy of 5.0 Bev.

Fig. 9. Neutron total and reaction cross sections for Pb, Cu, Al, and C. Solid curves are theoretical total cross sections. Dashed curves are theoretical reaction cross sections. The circles are experimental measurements.

Fig. 10. Neutron total and reaction cross sections for hydrogen. Solid curve is the theoretical cross section. The points are the experimental data for this experiment, together with statistical errors.

Fig. 11. Diffraction model of Greider and Glassgold. Dashed line gives the black-sphere model.

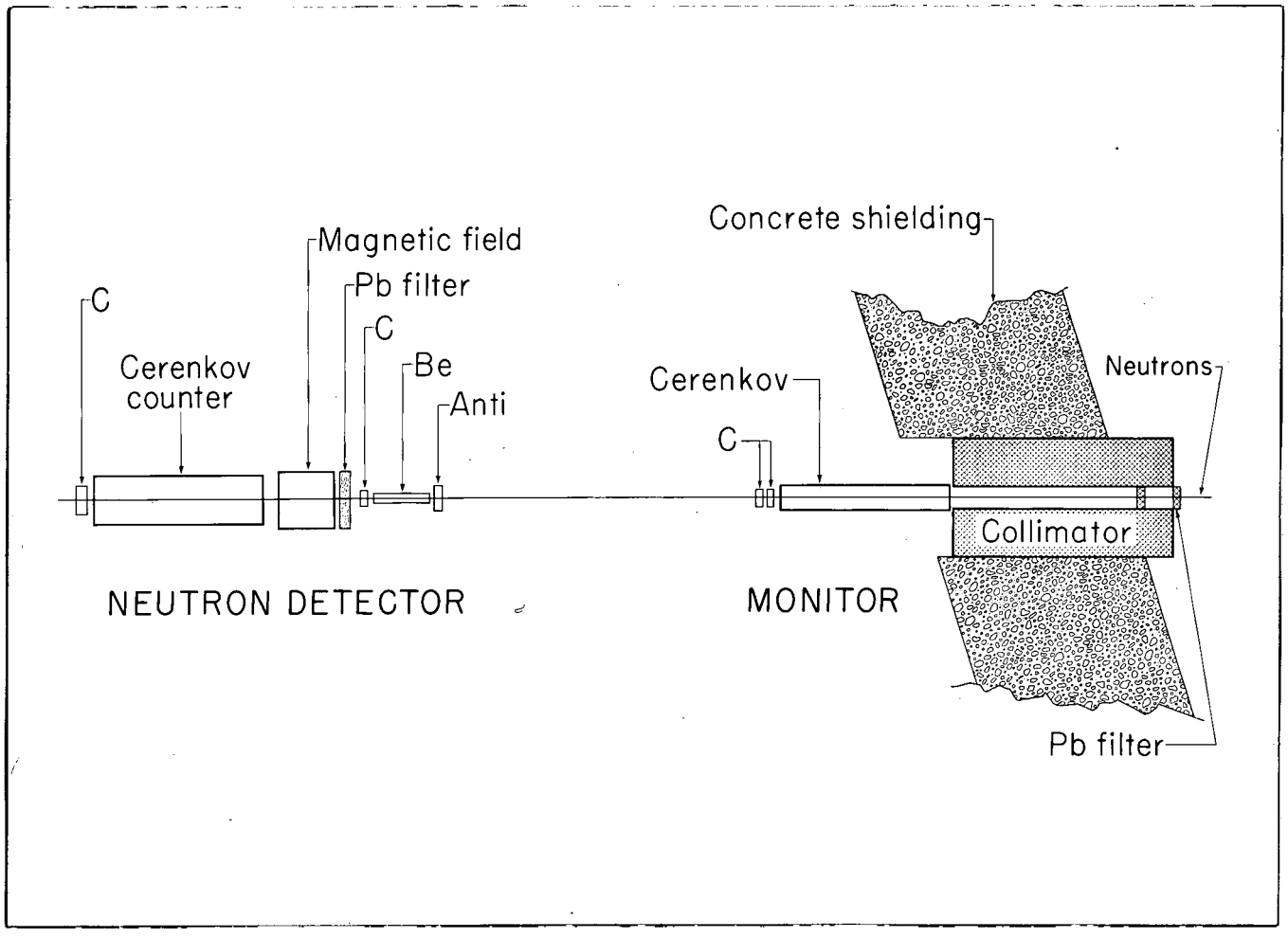
Concrete shielding
Magnetic field
Pb filter
C
C
Be
Anti
Cerenkov counter
Cerenkov
C
Neutrons
Collimator
NEUTRON DETECTOR
MONITOR
Pb filter

Fig. 1

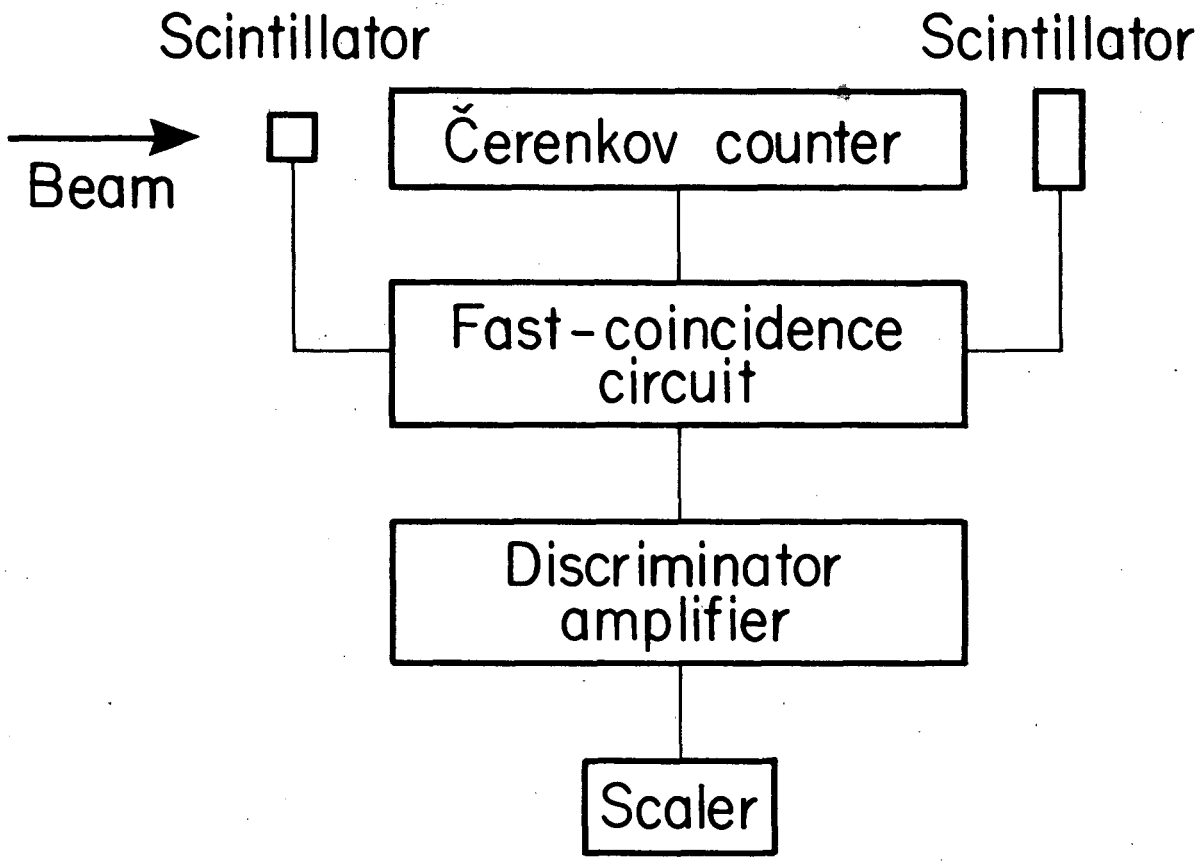

Figure 2

5-5227-1

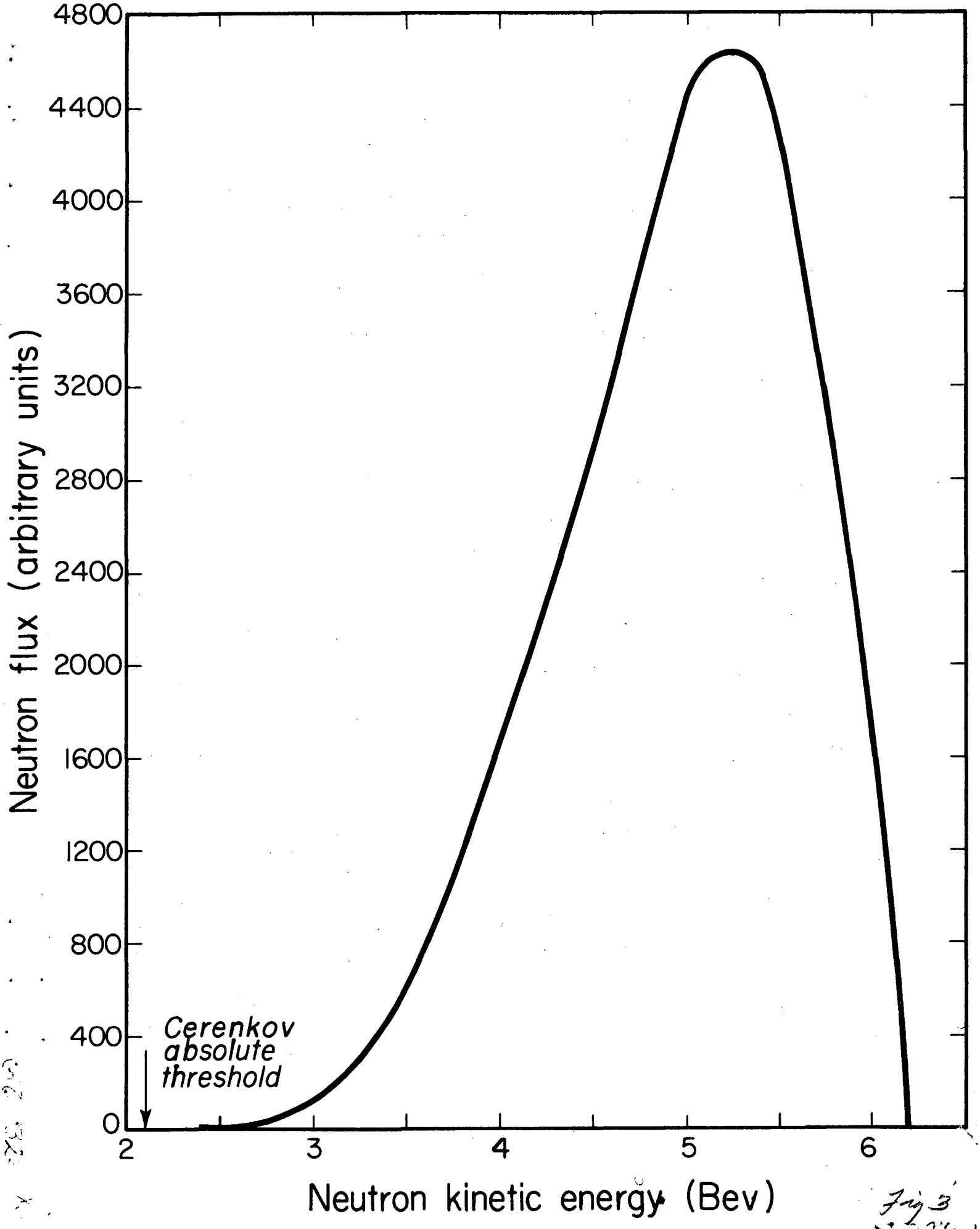
4800
4400
4000
3600
3200
2800
2400
2000
1600
1200
800
400
0
Neutron flux (arbitrary units)
Cerenkov
absolute
threshold
2
3
4
5
6
Neutron kinetic energy (Bev)

Fig 3
56-326-1

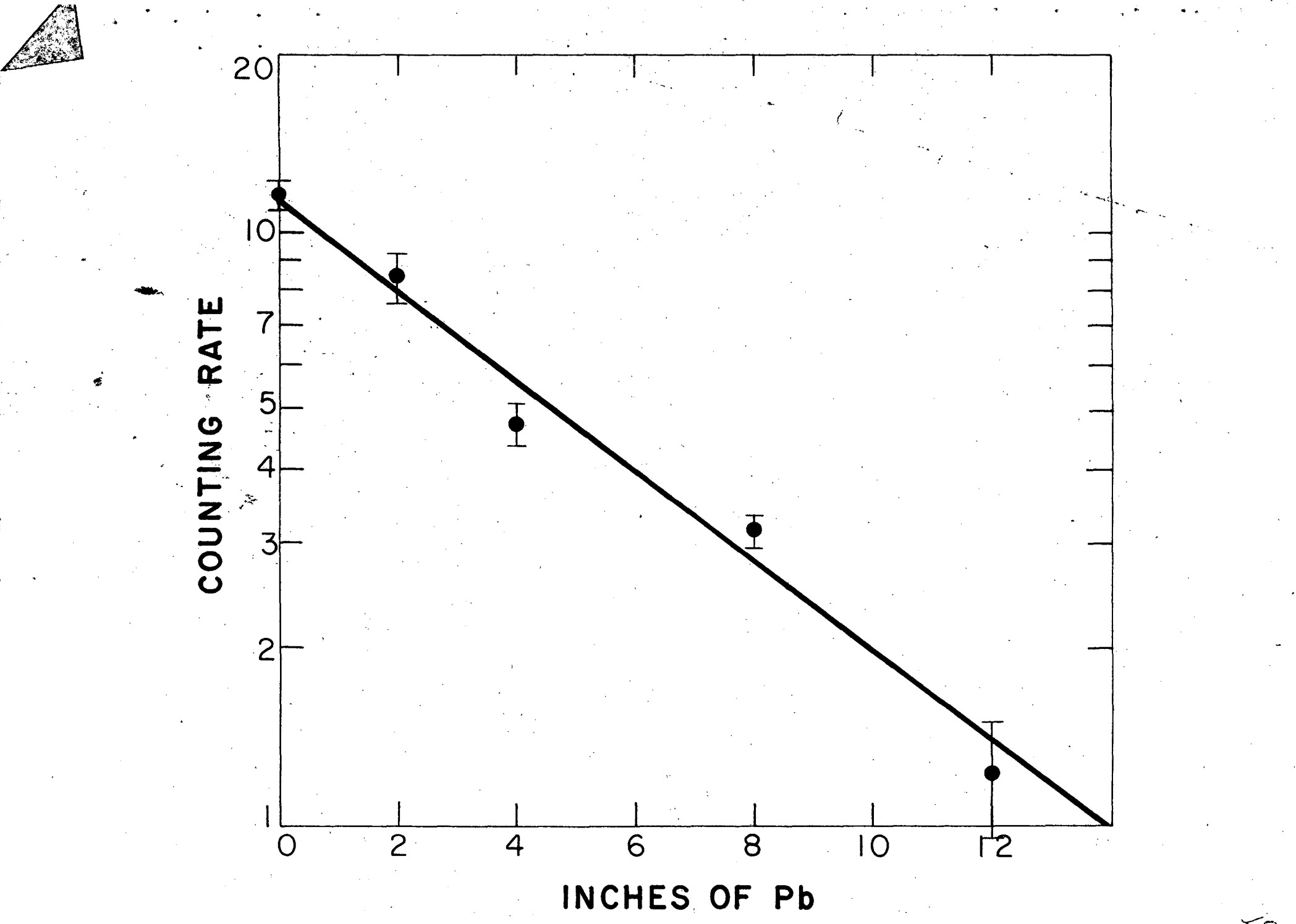

Fig. 53

50,754-1

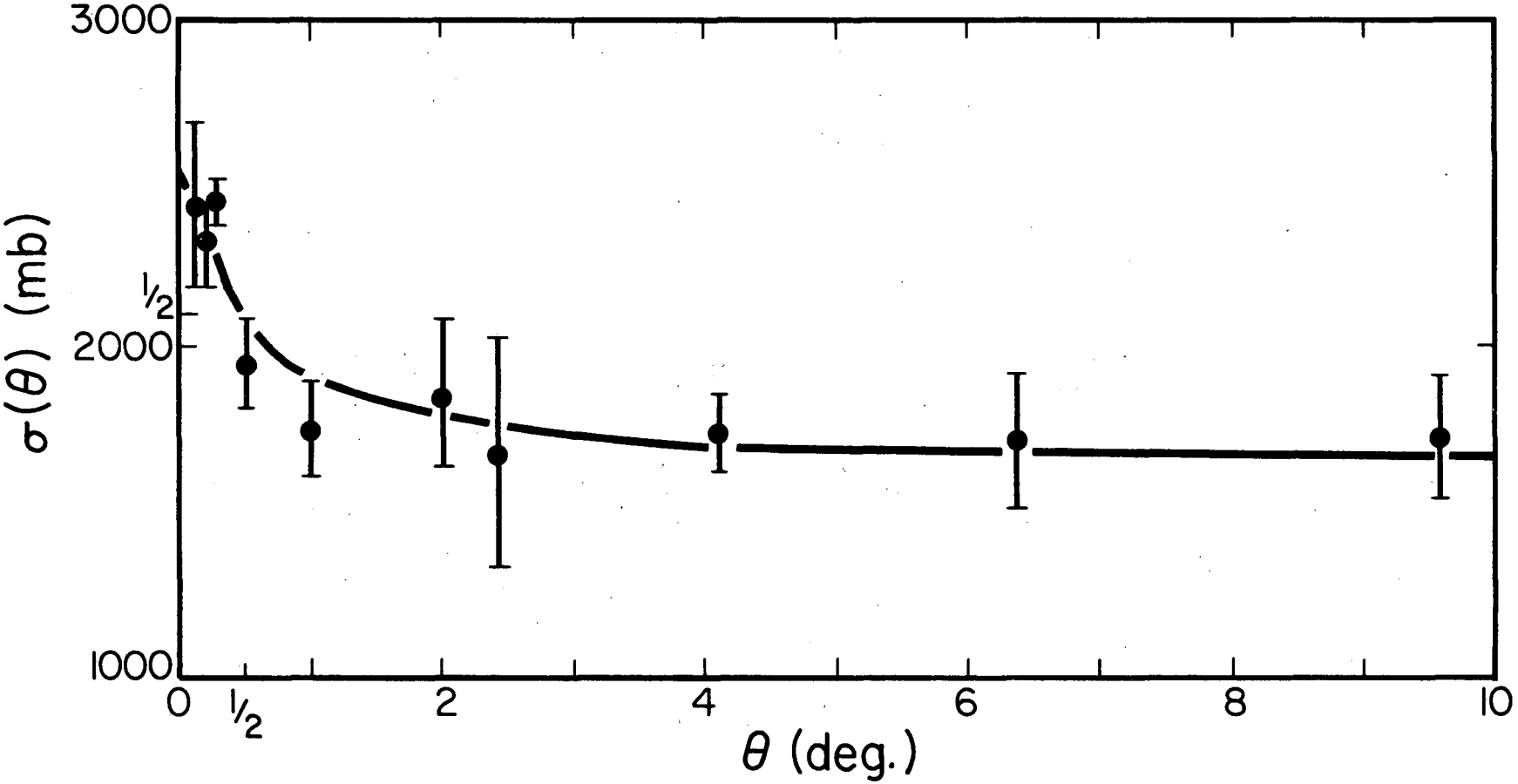

Fig 5
56 351-1

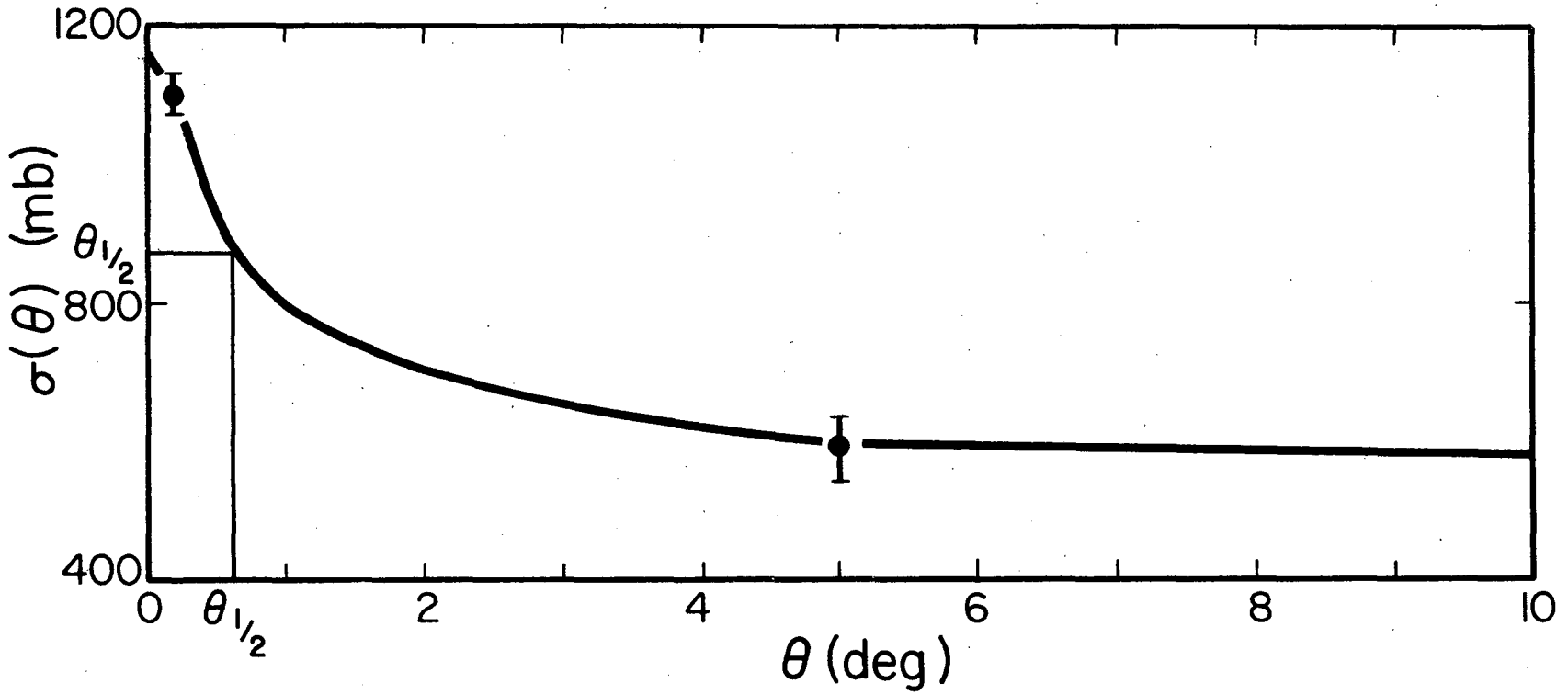

Fig 6

56332-1

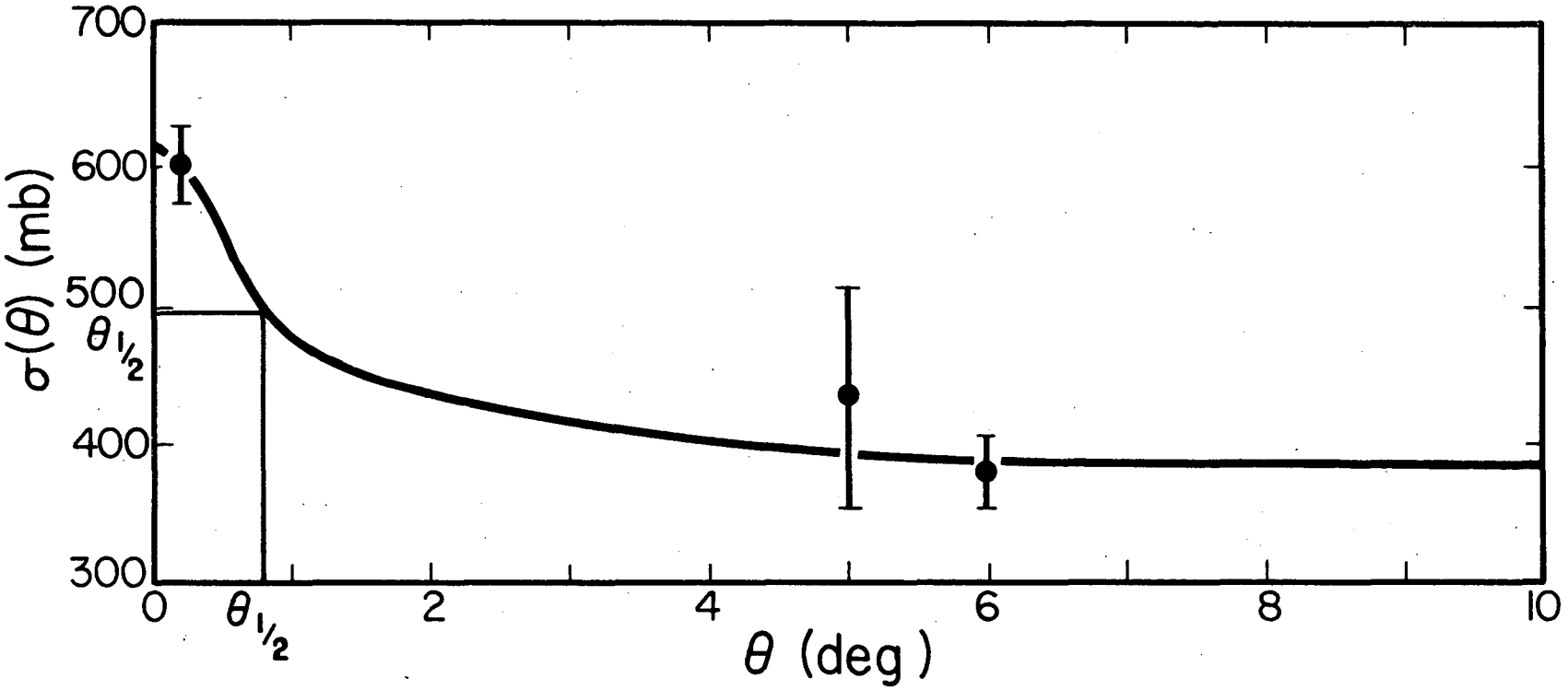

Fig 7
SL-333-1

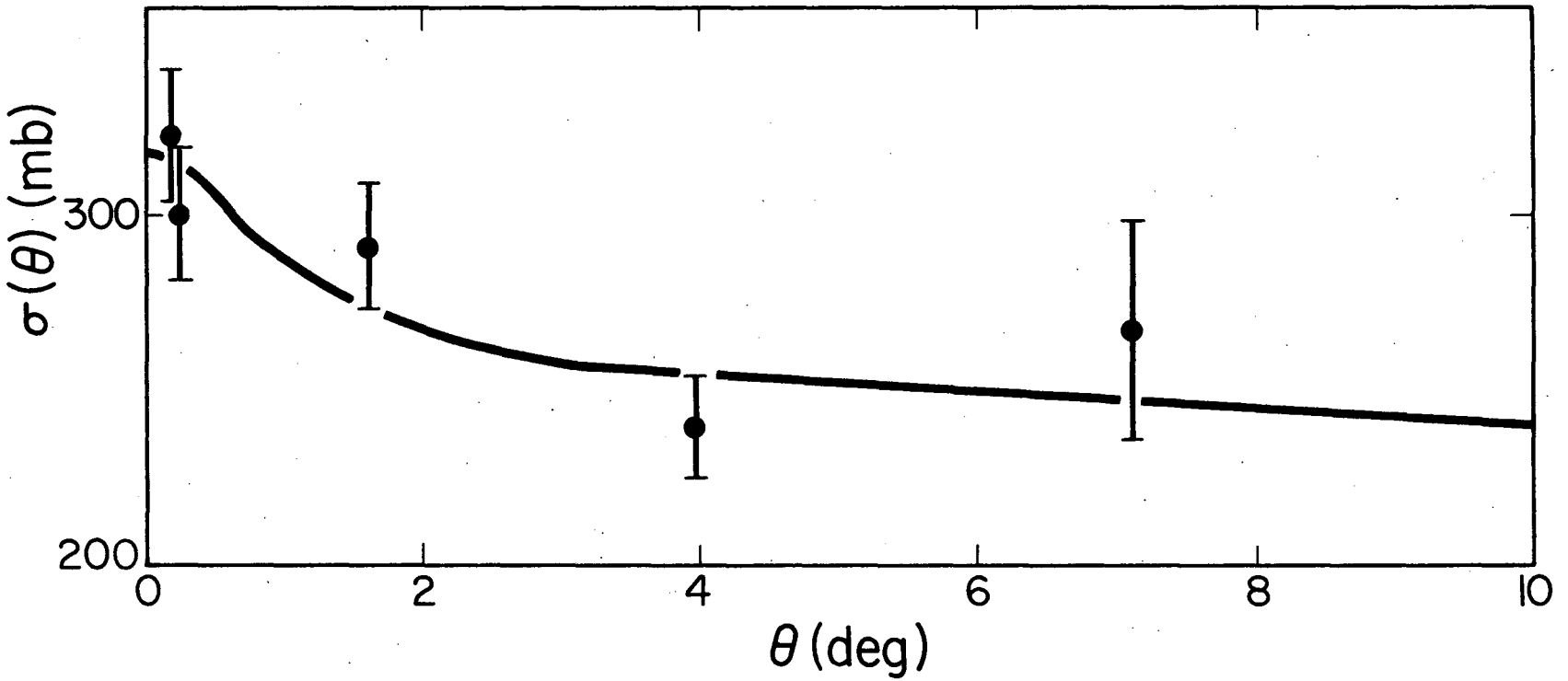

Fig 8
5633 4-1

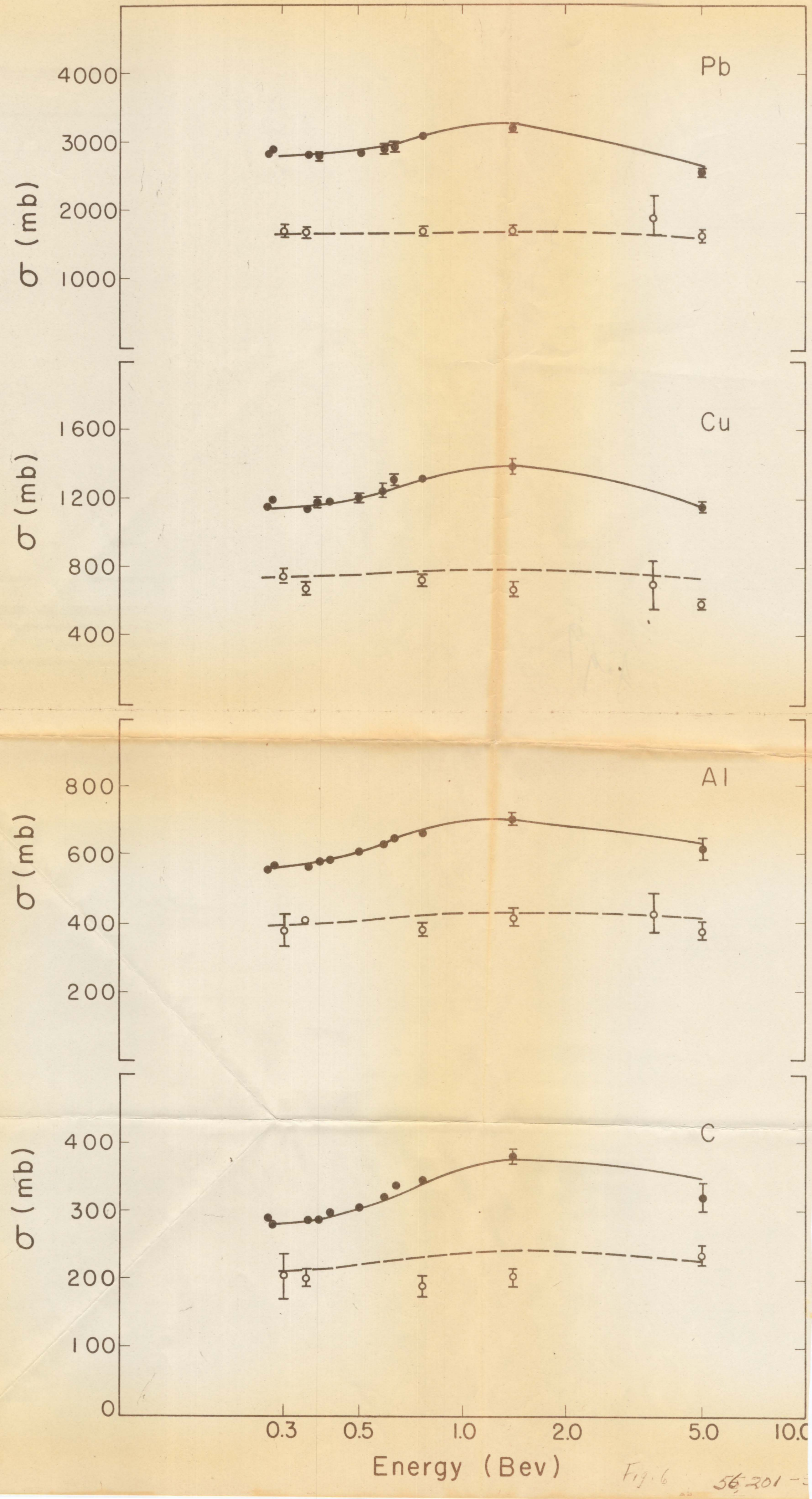
Pb
Cu
Al
C
σ (mb)
4000
3000
2000
1000
1600
1200
800
400
600
200
300
100
0
0.3
0.5
1.0
2.0
5.0
10.0
Energy (Bev)

Fig. 6

56-201-3

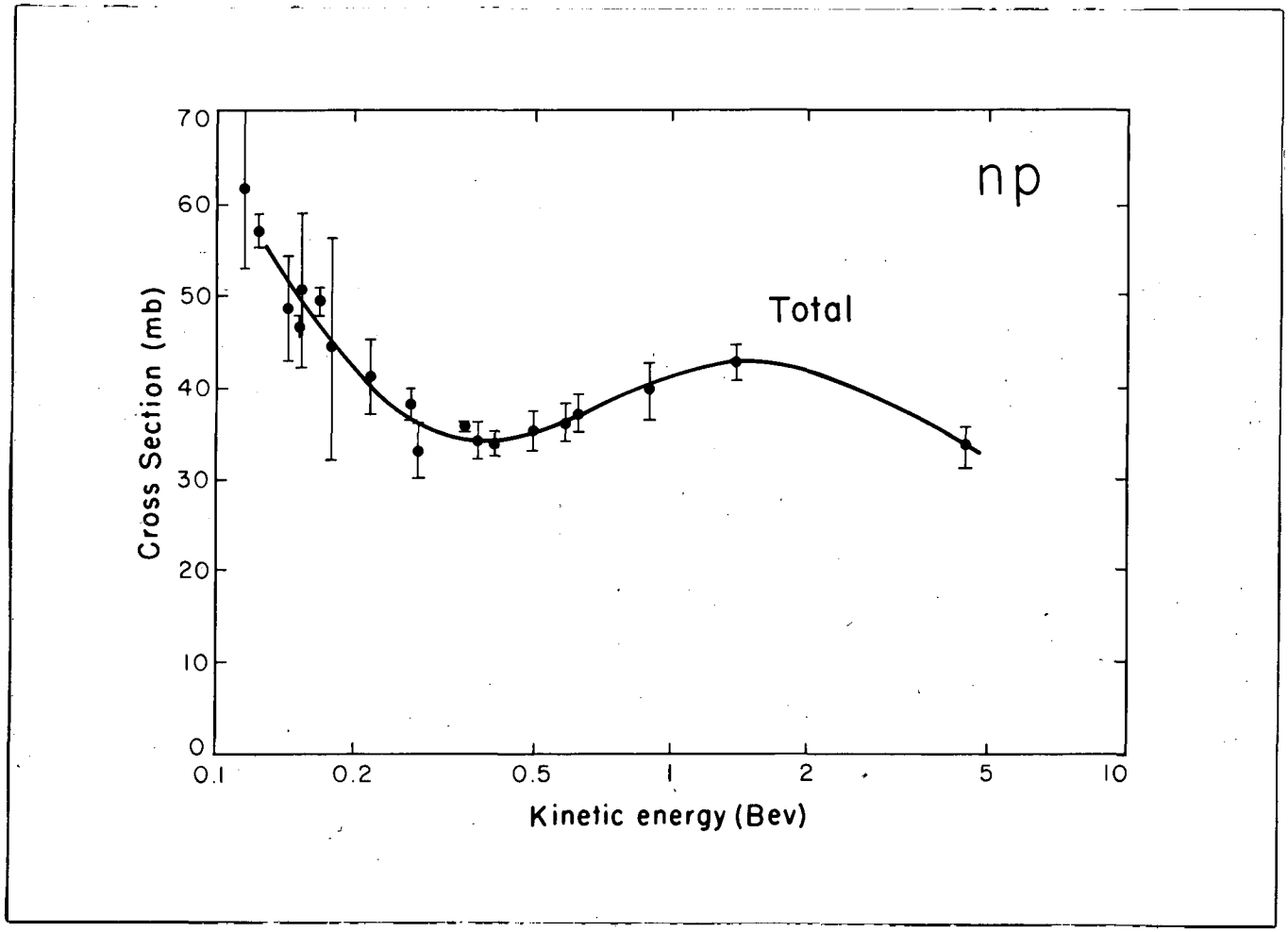
np
Total
Cross Section (mb)
Kinetic energy (Bev)
70
60
50
40
30
20
10
0
0.1
0.2
0.5
1
2
5
10

Fig. 10

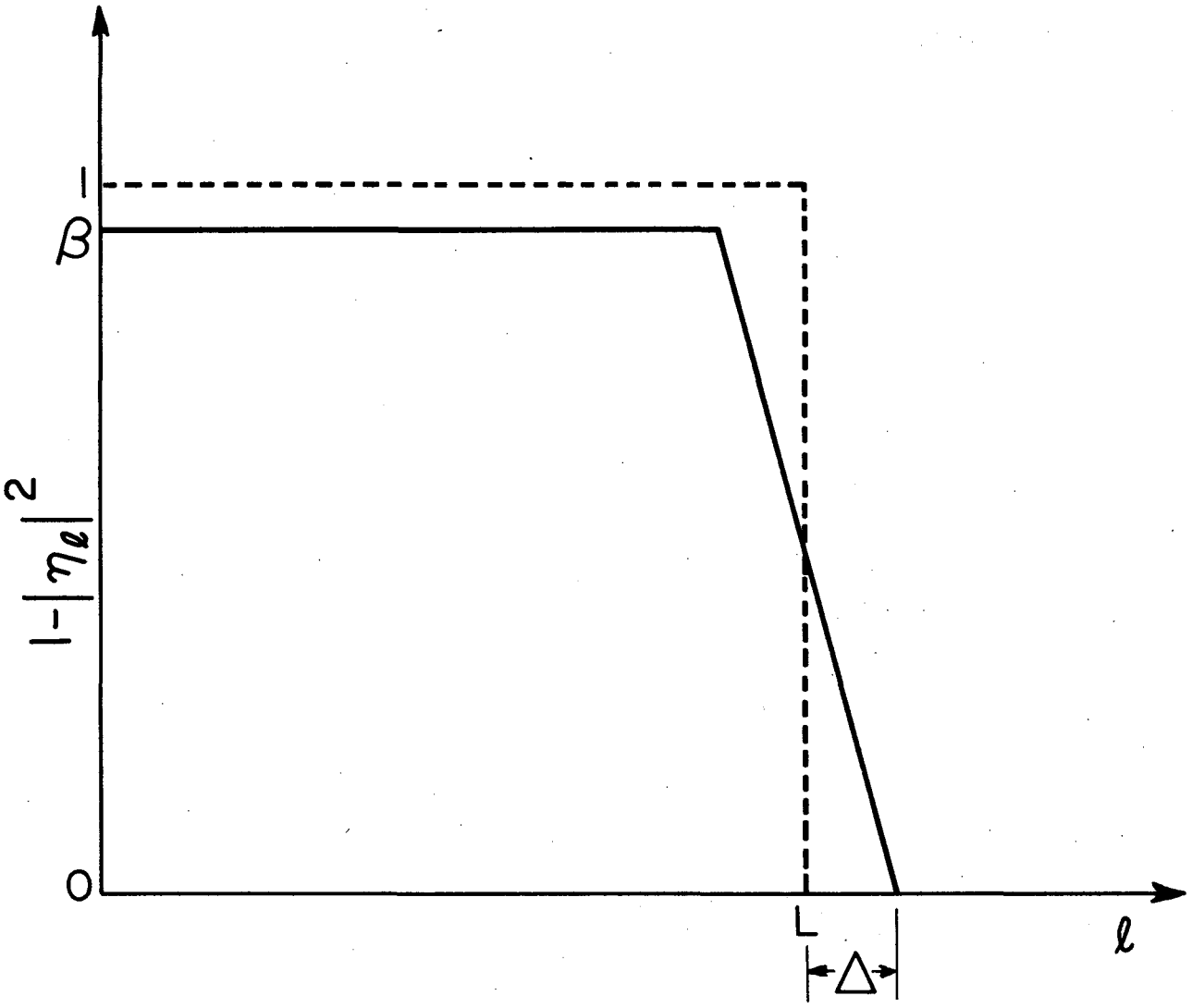

Fig 11
56 519-1

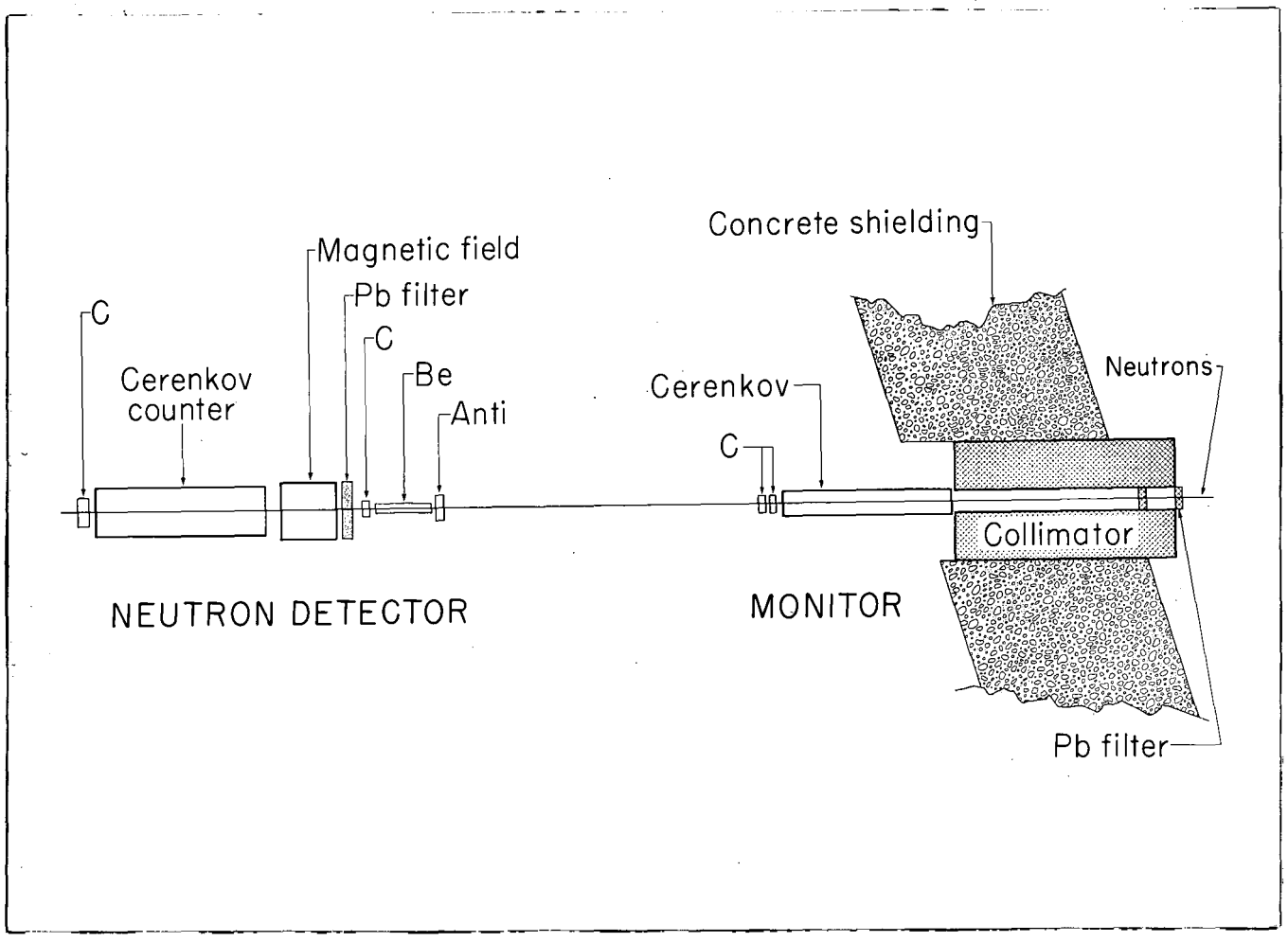
Concrete shielding
Magnetic field
Pb filter
C
C
Be
Anti
Cerenkov
counter
Cerenkov
C
Neutrons
Collimator
NEUTRON DETECTOR
MONITOR
Pb filter

Fig. 1

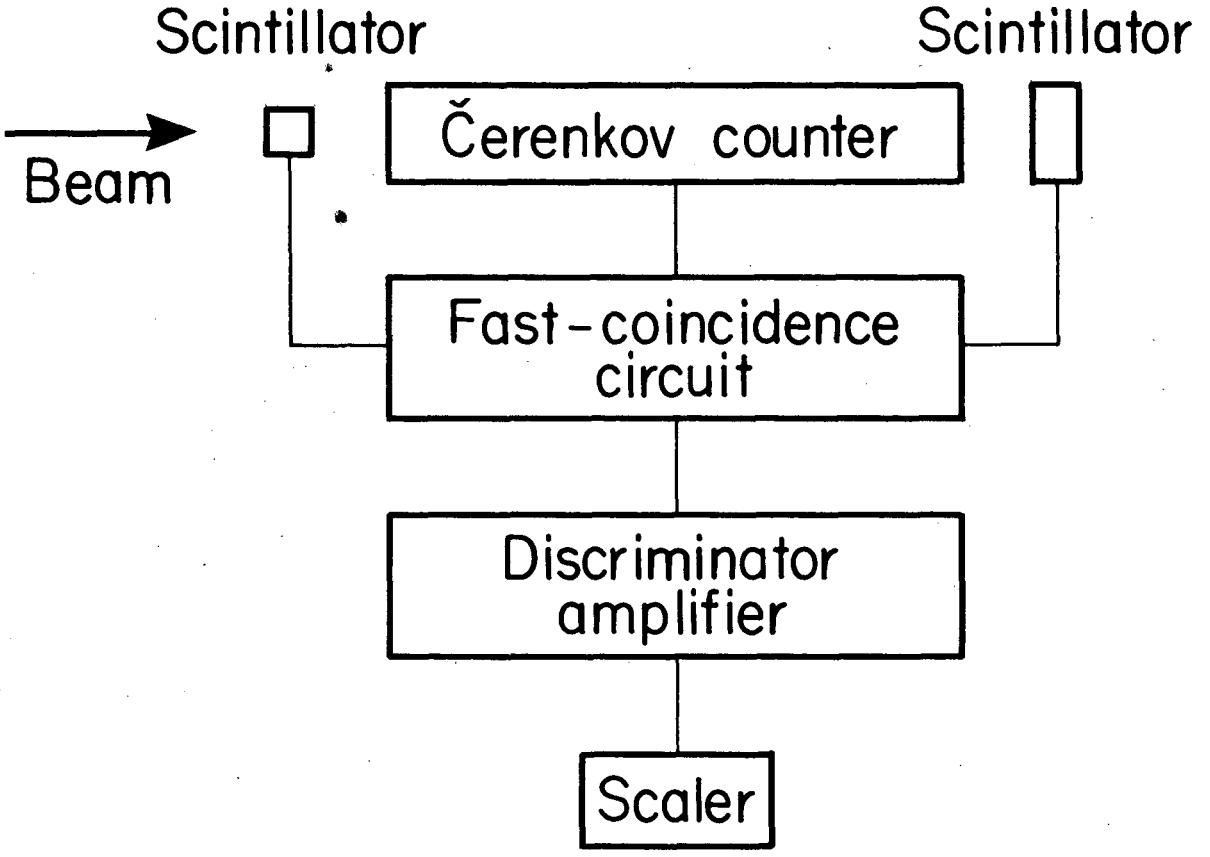

Figure 2
S-3226-1

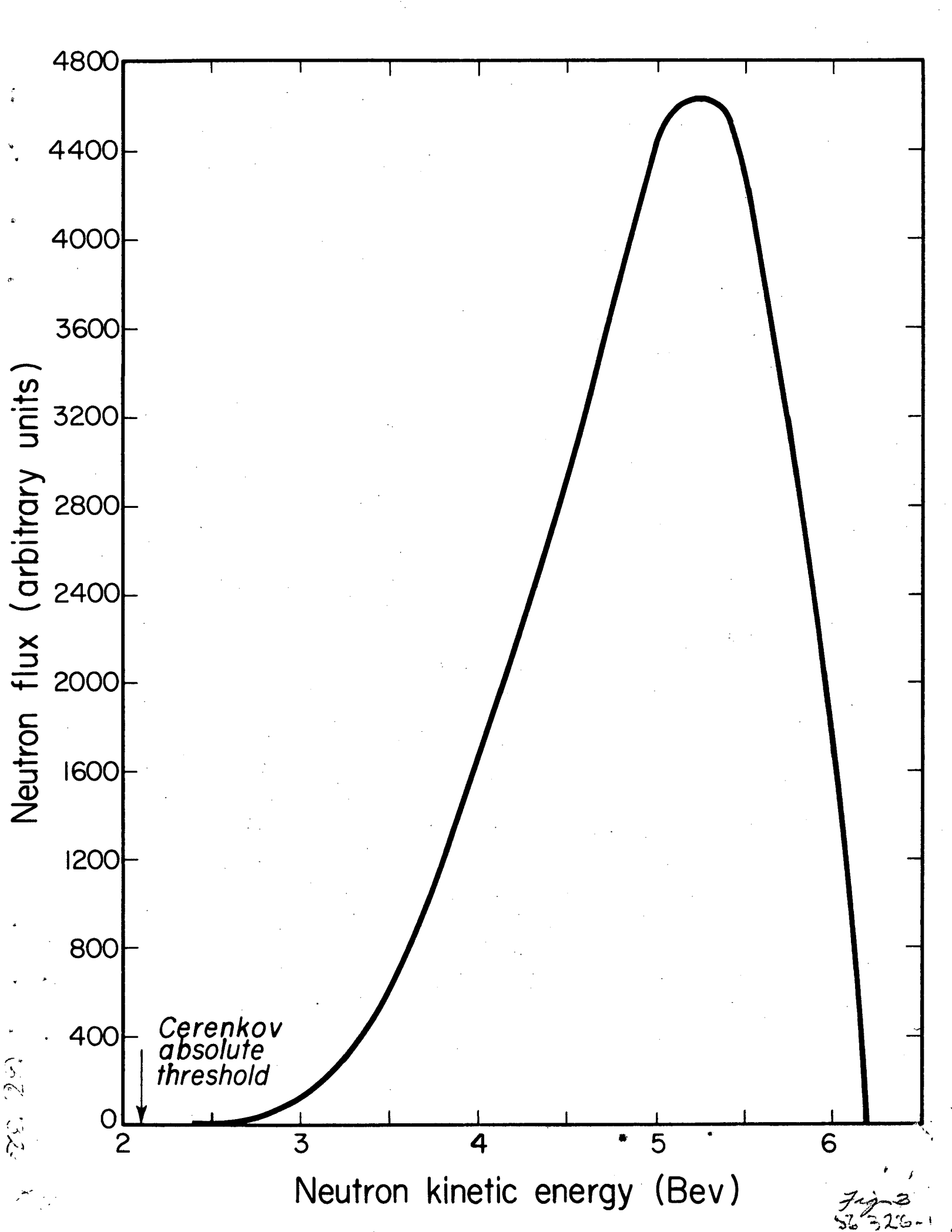
4800
4400
4000
3600
3200
2800
2400
2000
1600
1200
800
400
0
Neutron flux (arbitrary units)
Cerenkov
absolute
threshold
2
3
4
5
6
Neutron kinetic energy (Bev)

Fig-3
56 326-1

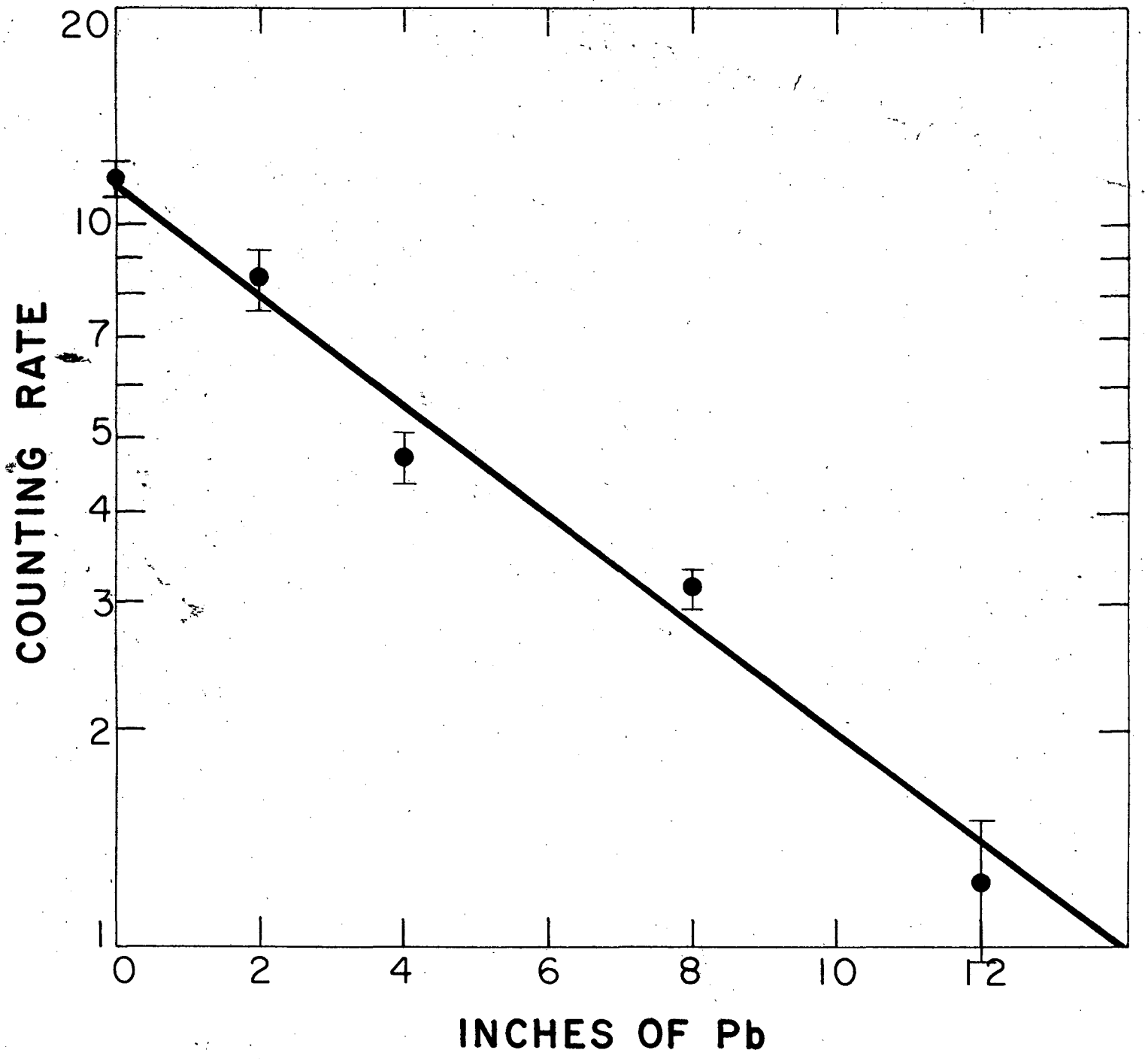

Fig. 53

50,754-1

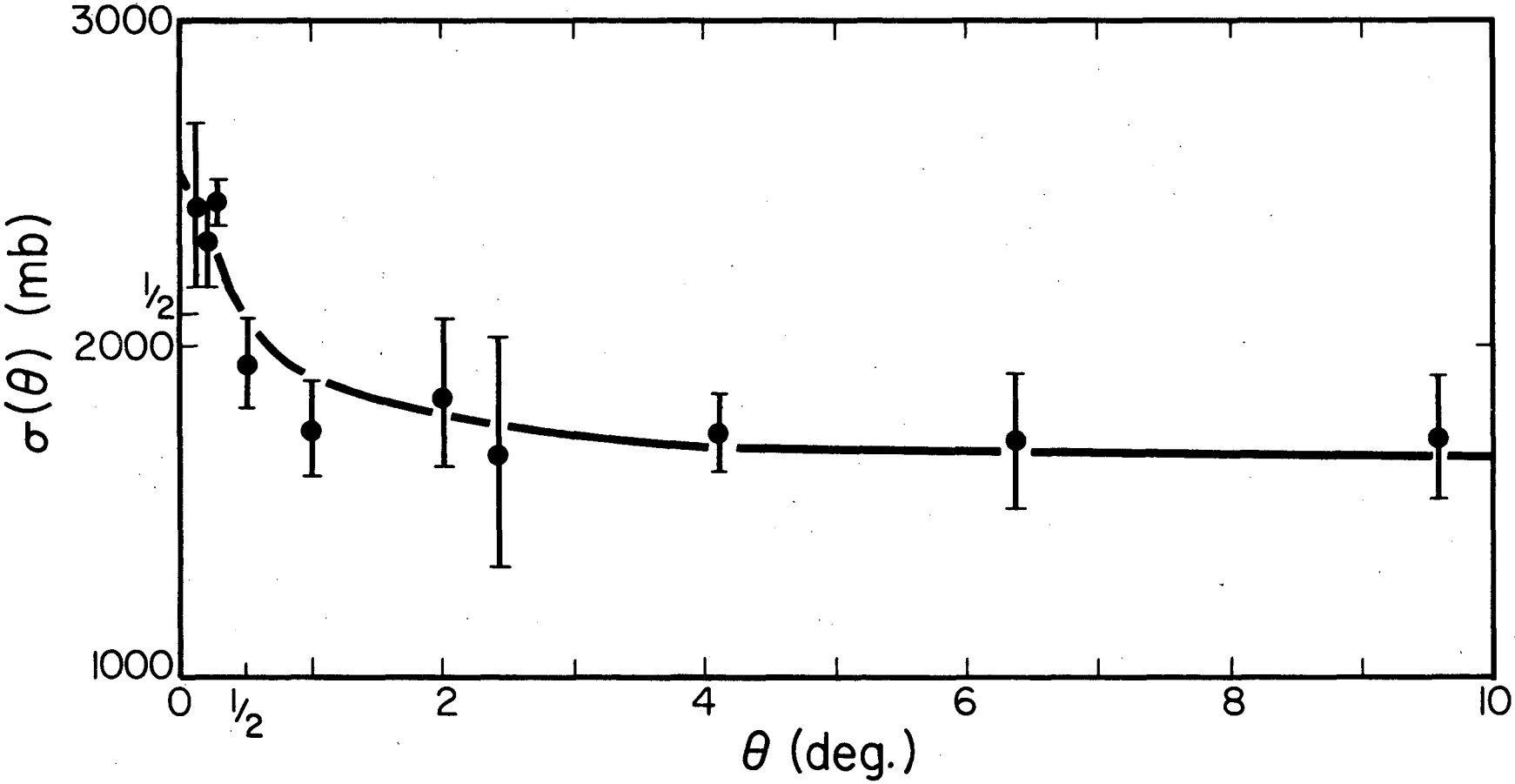

Fig 5

56-331-1

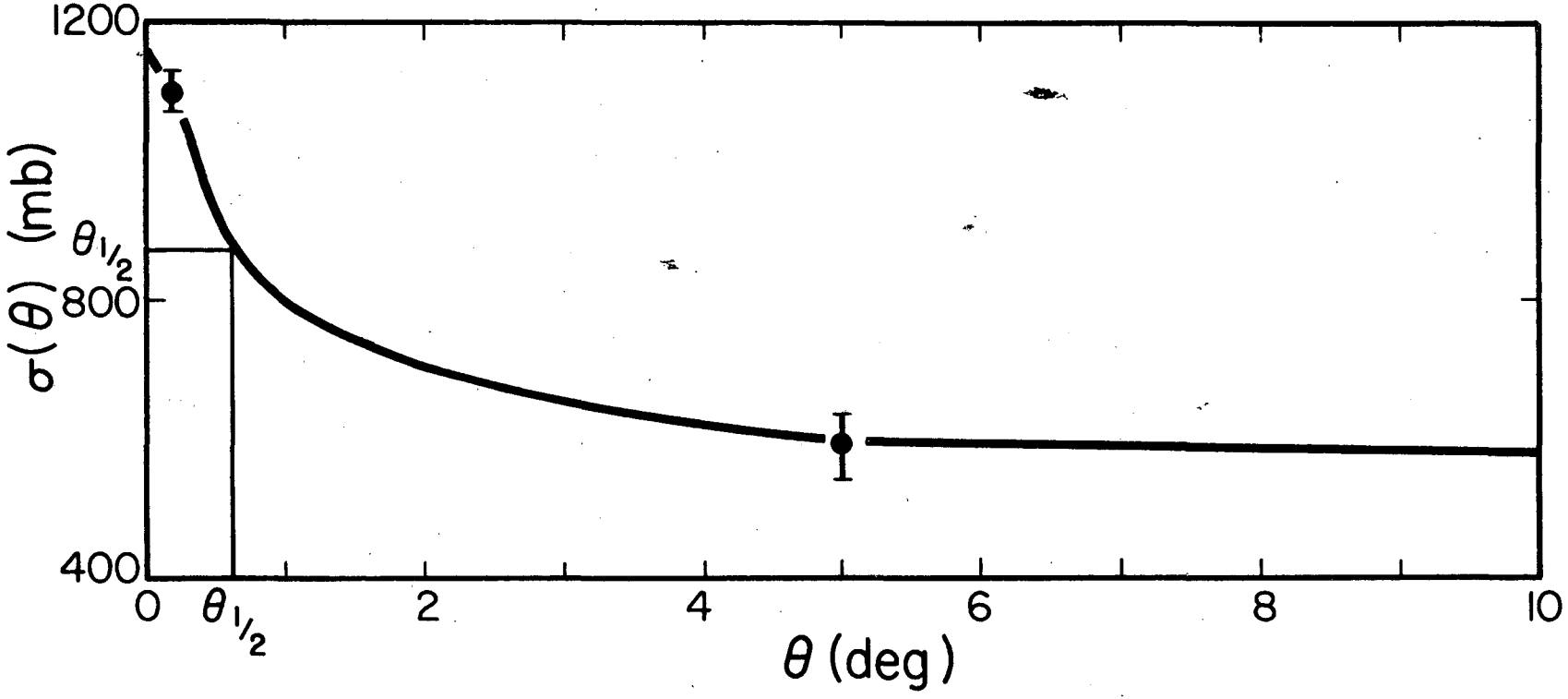

Fig. 6
56332-1

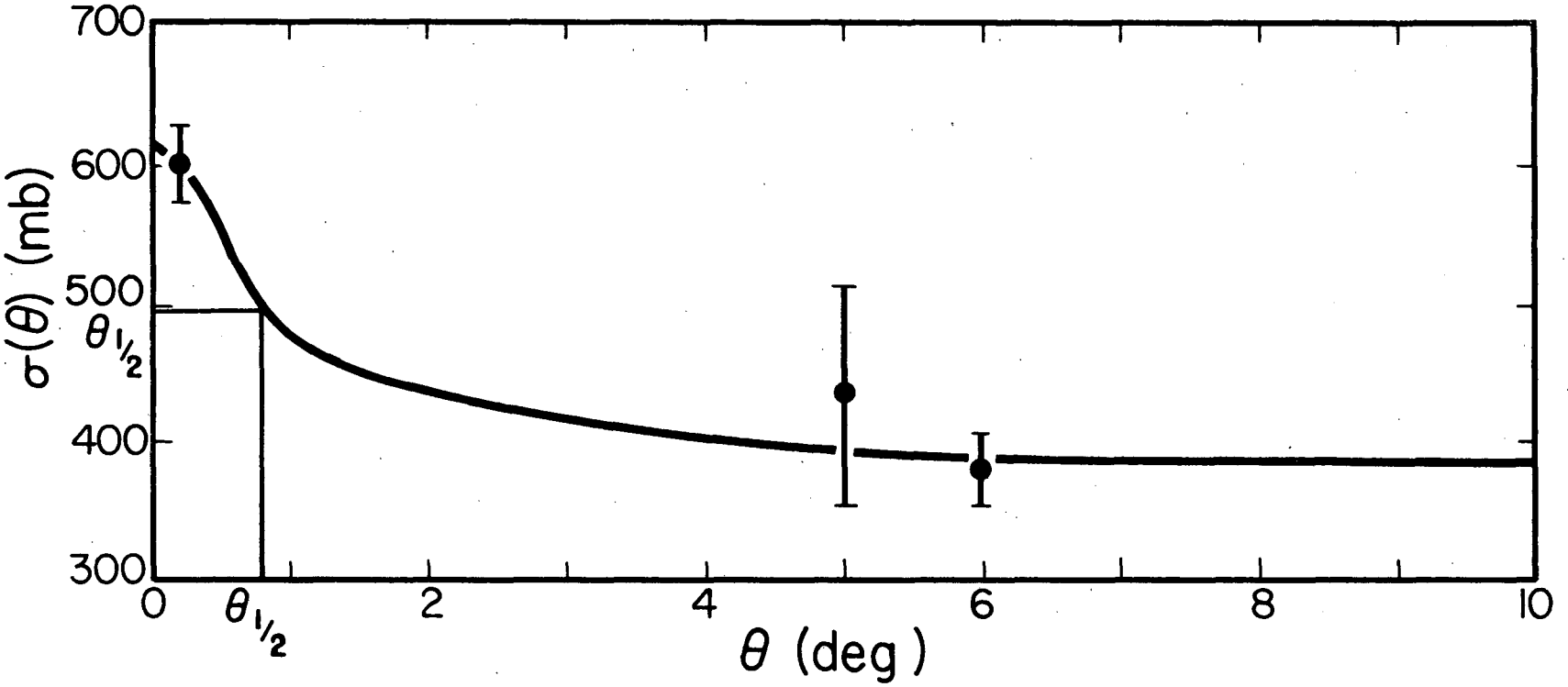

Fig 7

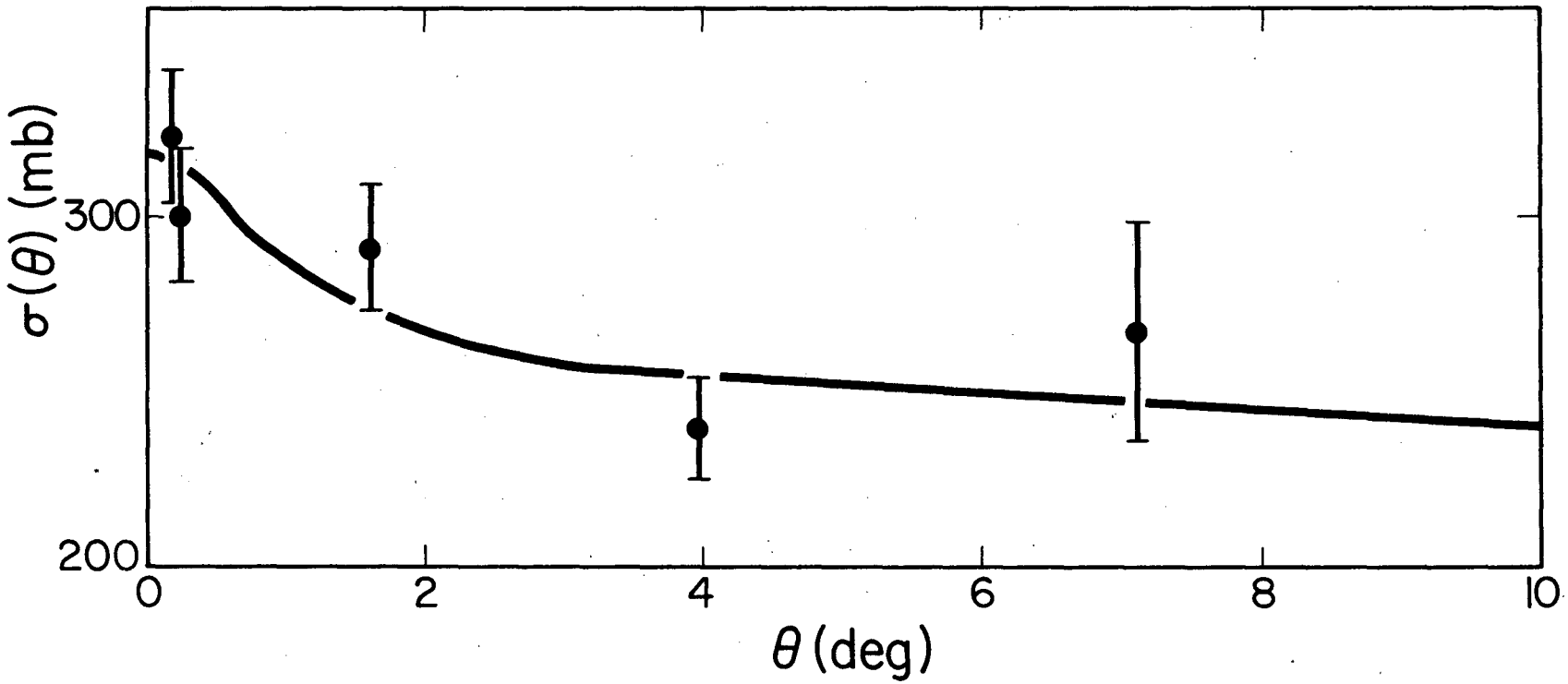

Fig 8
5635 4-1

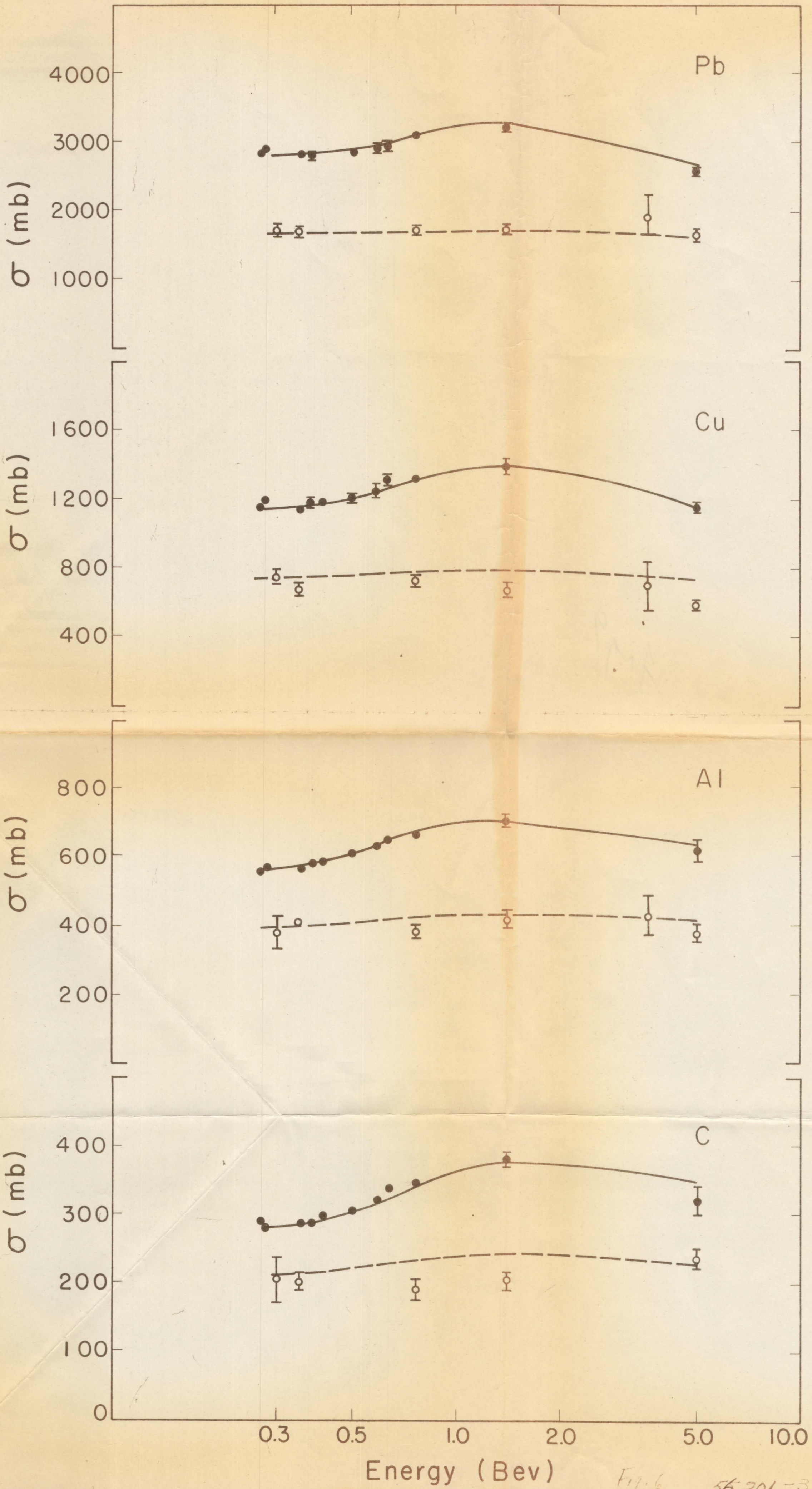
Pb
Cu
Al
C
σ (mb)
4000
3000
2000
1000
1600
1200
800
400
800
600
400
200
400
300
200
100
0
0.3
0.5
1.0
2.0
5.0
10.0
Energy (Bev)

Fig. 6

56-201-3

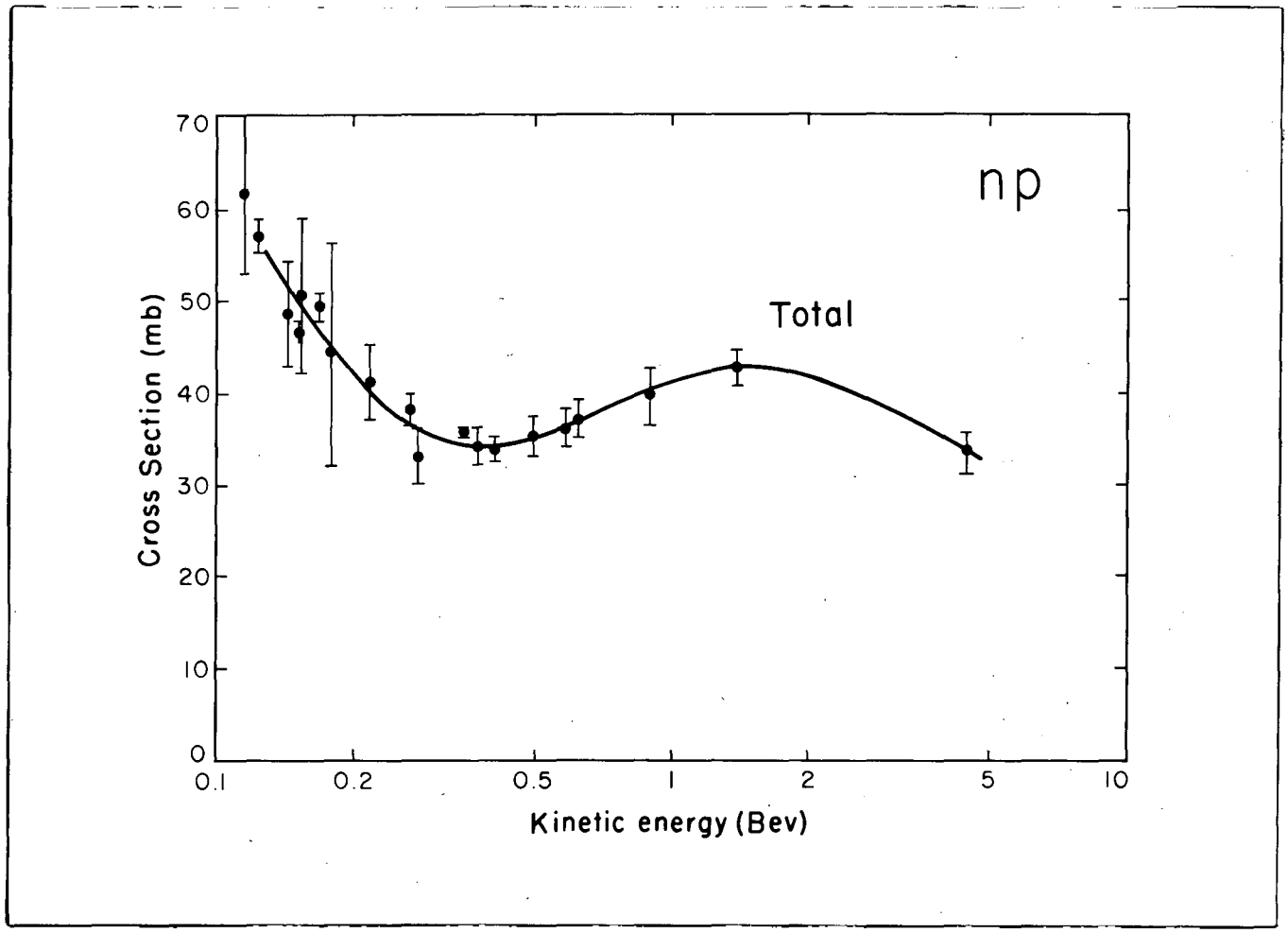
np
Total
Cross Section (mb)
Kinetic energy (Bev)
70
60
50
40
30
20
10
0
0.1
0.2
0.5
1
2
5
10

Fig. 10

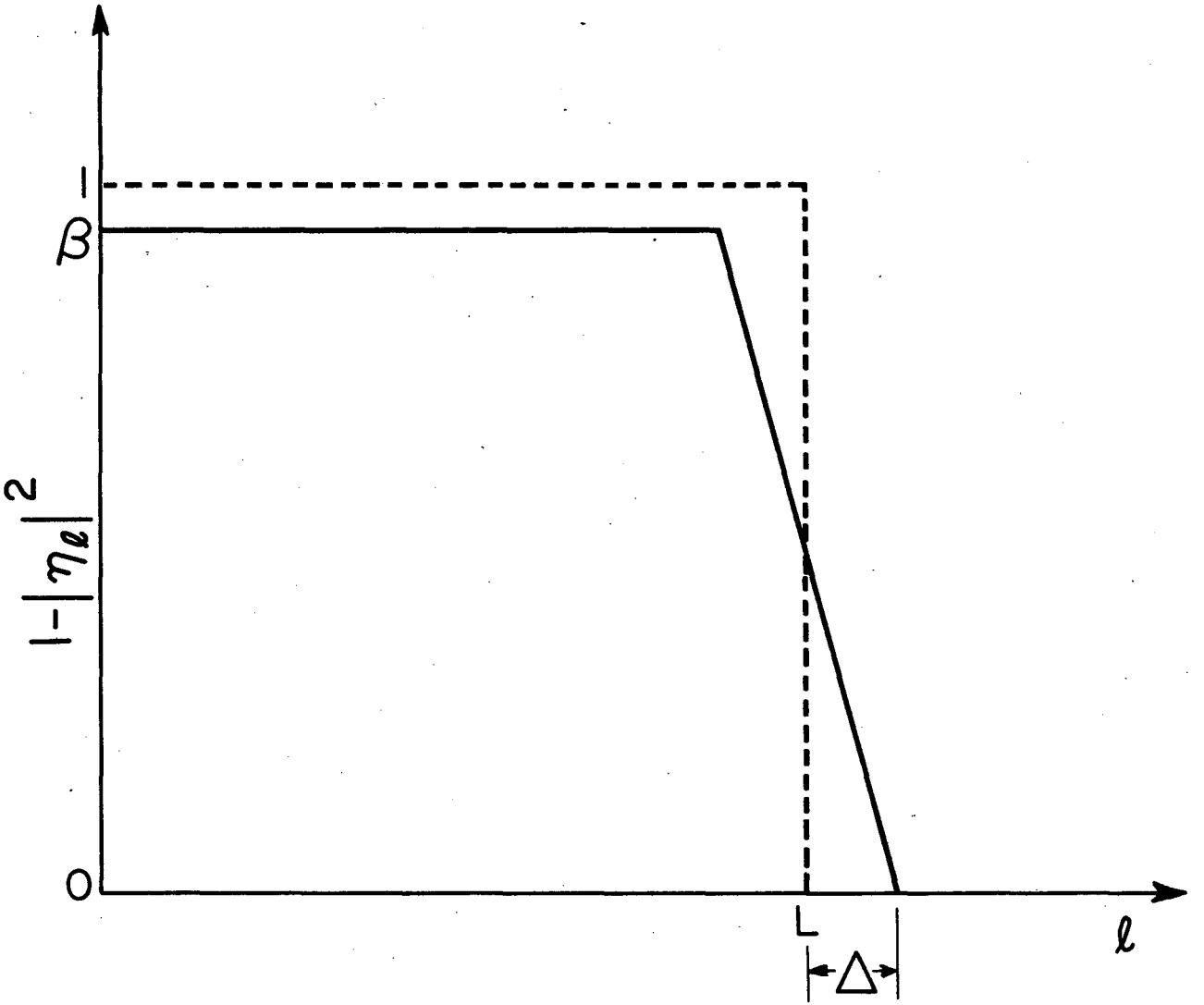

Fig 11
-5631 9-1